The Astrophysical Journal, 932:133 (27pp), 2022 June 20 https://doi.org/10.3847/1538-4357/ac6ad0

Narrowband Searches for Continuous and Long-duration Transient Gravitational Waves from Known Pulsars in the LIGO-Virgo Third Observing Run

R. Abbott[1], T. D. Abbott[2], F. Acernese[3,4], K. Ackley[5], C. Adams[6], N. Adhikari[7], R. X. Adhikari[1], V. B. Adya[8], C. Affeldt[9,10], D. Agarwal[11], M. Agathos[12,13], K. Agatsuma[14], N. Aggarwal[15], O. D. Aguiar[16], L. Aiello[17], A. Ain[18], P. Ajith[19], T. Akutsu[20,21], S. Albanesi[22], A. Allocca[4,23], P. A. Altin[8], A. Amato[24], C. Anand[5], S. Anand[1], A. Ananyeva[1], S. B. Anderson[1], W. G. Anderson[7], M. Ando[25,26], T. Andrade[27], N. Andres[28], T. Andrić[29], S. V. Angelova[30], S. Ansoldi[31,32], J. M. Antelis[33], S. Antier[34], S. Appert[1], Koji Arai[1], Koya Arai[35], Y. Arai[35], S. Araki[36], A. Araya[37], M. C. Araya[1], J. S. Areeda[38], M. Arène[34], N. Aritomi[25], N. Arnaud[39,40], S. M. Aronson[2], K. G. Arun[41], H. Asada[42], Y. Asali[43], G. Ashton[5], Y. Aso[44,45], M. Assiduo[46,47], S. M. Aston[6], P. Astone[48], F. Aubin[28], C. Austin[2], S. Babak[34], F. Badaracco[49], M. K. M. Bader[50], C. Badger[51], S. Bae[52], Y. Bae[53], A. M. Baer[54], S. Bagnasco[22], Y. Bai[1], M. Bailes[55], L. Baiotti[56], J. Baird[34], R. Bajpai[57], M. Ball[58], G. Ballardin[40], S. W. Ballmer[59], A. Balsamo[54], G. Baltus[60], S. Banagiri[61], D. Bankar[11], J. C. Barayoga[1], C. Barbieri[62,63,64], B. C. Barish[1], D. Barker[65], P. Barneo[27], F. Barone[4,66], B. Barr[67], L. Barsotti[68], M. Barsuglia[34], D. Barta[69], J. Bartlett[65], M. A. Barton[20,67], I. Bartos[70], R. Bassiri[71], A. Basti[18,72], M. Bawaj[73,74], J. C. Bayley[67], A. C. Baylor[7], M. Bazzan[75,76], B. Bécsy[77], V. M. Bedakihale[78], M. Bejger[79], I. Belahcene[39], V. Benedetto[80], D. Beniwal[81], T. F. Bennett[82], J. D. Bentley[14], M. BenYaala[30], F. Bergamin[9,10], B. K. Berger[71], S. Bernuzzi[13], D. Bersanetti[83], A. Bertolini[50], J. Betzwieser[6], D. Beveridge[84], R. Bhandare[85], U. Bhardwaj[50,86], D. Bhattacharjee[87], S. Bhaumik[70], I. A. Bilenko[88], G. Billingsley[1], S. Bini[89,90], R. Birney[91], O. Birnholtz[92], S. Biscans[1,68], M. Bischi[46,47], S. Biscoveanu[68], A. Bisht[9,10], B. Biswas[11], M. Bitossi[18,40], M.-A. Bizouard[93], J. K. Blackburn[1], C. D. Blair[6,84], D. G. Blair[84], R. M. Blair[65], F. Bobba[94,95], N. Bode[9,10], M. Boer[93], G. Bogaert[93], M. Boldrini[48,96], L. D. Bonavena[75], F. Bondu[97], E. Bonilla[71], R. Bonnand[28], P. Booker[9,10], B. A. Boom[50], R. Bork[1], V. Boschi[18], N. Bose[98], S. Bose[11], V. Bossilkov[84], V. Boudart[60], Y. Bouffanais[75,76], A. Bozzi[40], C. Bradaschia[18], P. R. Brady[7], A. Bramley[6], A. Branch[6], M. Branchesi[29,99], J. E. Brau[58], M. Breschi[13], T. Briant[100], J. H. Briggs[67], A. Brillet[93], M. Brinkmann[9,10], P. Brockill[7], A. F. Brooks[1], J. Brooks[40], D. D. Brown[81], S. Brunett[1], G. Bruno[49], R. Bruntz[54], J. Bryant[14], T. Bulik[101], H. J. Bulten[50], A. Buonanno[102,103], R. Buscicchio[14], D. Buskulic[28], C. Buy[104], R. L. Byer[71], L. Cadonati[105], G. Cagnoli[24], C. Cahillane[65], J. Calderón Bustillo[106,107], J. D. Callaghan[67], T. A. Callister[108,109], E. Calloni[4,23], J. Cameron[84], J. B. Camp[110], M. Canepa[83,111], S. Canevarolo[112], M. Cannavacciuolo[94], K. C. Cannon[113], H. Cao[81], Z. Cao[114], E. Capocasa[20], E. Capote[59], G. Carapella[94,95], F. Carbognani[40], J. B. Carlin[115], M. F. Carney[15], M. Carpinelli[40,116,117], G. Carrillo[58], G. Carullo[18,72], T. L. Carver[17], J. Casanueva Diaz[40], C. Casentini[118,119], G. Castaldi[120], S. Caudill[50,112], M. Cavaglià[87], F. Cavalier[39], R. Cavalieri[40], M. Ceasar[121], G. Cella[18], P. Cerdá-Durán[122], E. Cesarini[119], W. Chaibi[93], K. Chakravarti[11], S. Chalathadka Subrahmanya[123], E. Champion[124], C.-H. Chan[125], C. Chan[113], C. L. Chan[107], K. Chan[107], M. Chan[126], K. Chandra[98], P. Chanial[40], S. Chao[125], P. Charlton[127], E. A. Chase[15], E. Chassande-Mottin[34], C. Chatterjee[84], Debarati Chatterjee[11], Deep Chatterjee[7], M. Chaturvedi[85], S. Chaty[34], C. Chen[128,129], H. Y. Chen[68], J. Chen[125], K. Chen[130], X. Chen[84], Y.-B. Chen[131], Y.-R. Chen[132], Z. Chen[17], H. Cheng[70], C. K. Cheong[107], H. Y. Cheung[107], H. Y. Chia[70], F. Chiadini[95,133], C-Y. Chiang[134], G. Chiarini[76], R. Chierici[135], A. Chincarini[83], M. L. Chiofalo[18,72], A. Chiummo[40], G. Cho[136], H. S. Cho[137], R. K. Choudhary[84], S. Choudhary[11], N. Christensen[93], H. Chu[130], Q. Chu[84], Y-K. Chu[134], S. Chua[8], K. W. Chung[51], G. Ciani[75,76], P. Ciecielag[79], M. Cieślar[79], M. Cifaldi[118,119], A. A. Ciobanu[81], R. Ciolfi[76,138], F. Cipriano[93], A. Cirone[83,111], F. Clara[65], E. N. Clark[139], J. A. Clark[1,105], L. Clarke[140], P. Clearwater[55], S. Clesse[141], F. Cleva[93], E. Coccia[29,99], E. Codazzo[29], P.-F. Cohadon[100], D. E. Cohen[39], L. Cohen[2], M. Colleoni[142], C. G. Collette[143], A. Colombo[62], M. Colpi[62,63], C. M. Compton[65], M. Constancio, Jr.[16], L. Conti[76], S. J. Cooper[14], P. Corban[6], T. R. Corbitt[2], I. Cordero-Carrión[144], S. Corezzi[73,74], K. R. Corley[43], N. Cornish[77], D. Corre[39], A. Corsi[145], S. Cortese[40], C. A. Costa[16], R. Cotesta[103], M. W. Coughlin[61], J.-P. Coulon[93], S. T. Countryman[43], B. Cousins[146], P. Couvares[1], D. M. Coward[84], M. J. Cowart[6], D. C. Coyne[1], R. Coyne[147], J. D. E. Creighton[7], T. D. Creighton[148], A. W. Criswell[61], M. Croquette[100], S. G. Crowder[149], J. R. Cudell[60], T. J. Cullen[2], A. Cumming[67], R. Cummings[67], L. Cunningham[67], E. Cuoco[18,40,150], M. Curyło[101], P. Dabadie[24], T. Dal Canton[39], S. Dall'Osso[29], G. Dálya[151], A. Dana[71], L. M. DaneshgaranBajastani[82], B. D'Angelo[83,111], S. Danilishin[50,152], S. D'Antonio[119], K. Danzmann[9,10], C. Darsow-Fromm[123], A. Dasgupta[78], L. E. H. Datrier[67], S. Datta[11], V. Dattilo[40], I. Dave[85], M. Davier[39], G. S. Davies[153], D. Davis[1], M. C. Davis[121], E. J. Daw[154], R. Dean[121], D. DeBra[71], M. Deenadayalan[11], J. Degallaix[155], M. De Laurentis[4,23], S. Deléglise[100], V. Del Favero[124], F. De Lillo[49], N. De Lillo[67], W. Del Pozzo[18,72], L. M. DeMarchi[15], F. De Matteis[118,119], V. D'Emilio[17], N. Demos[68], T. Dent[106], A. Depasse[49], R. De Pietri[156,157], R. De Rosa[4,23], C. De Rossi[40], R. DeSalvo[120], R. De Simone[133], S. Dhurandhar[11], M. C. Díaz[148], M. Diaz-Ortiz, Jr.[70], N. A. Didio[59], T. Dietrich[50,103], L. Di Fiore[4], C. Di Fronzo[14], C. Di Giorgio[94,95], F. Di Giovanni[122], M. Di Giovanni[29], T. Di Girolamo[4,23], A. Di Lieto[18,72], B. Ding[143], S. Di Pace[48,96], I. Di Palma[48,96], F. Di Renzo[18,72], A. K. Divakarla[70], A. Dmitriev[14], Z. Doctor[58], L. D'Onofrio[4,23], F. Donovan[68], K. L. Dooley[17], S. Doravari[11], I. Dorrington[17], M. Drago[48,96], J. C. Driggers[65], Y. Drori[1], J.-G. Ducoin[39], P. Dupej[67], O. Durante[94,95], D. D'Urso[116,117], P.-A. Duverne[39], S. E. Dwyer[65], C. Eassa[65], P. J. Easter[5], M. Ebersold[158], T. Eckhardt[123], G. Eddolls[67], B. Edelman[58], T. B. Edo[1], O. Edy[153], A. Effler[6], S. Eguchi[126], J. Eichholz[8], S. S. Eikenberry[70], M. Eisenmann[28], R. A. Eisenstein[68], A. Ejlli[17], E. Engelby[38], Y. Enomoto[25], L. Errico[4,23], R. C. Essick[159], H. Estellés[142], D. Estevez[160], Z. Etienne[161], T. Etzel[1], M. Evans[68], T. M. Evans[6], B. E. Ewing[146], V. Fafone[29,118,119], H. Fair[59], S. Fairhurst[17], A. M. Farah[159], S. Farinon[83], B. Farr[58],

W. M. Farr[108,109], N. W. Farrow[5], E. J. Fauchon-Jones[17], G. Favaro[75], M. Favata[162], M. Fays[60], M. Fazio[163], J. Feicht[1], M. M. Fejer[71], E. Fenyvesi[69,164], D. L. Ferguson[165], A. Fernandez-Galiana[68], I. Ferrante[18,72], T. A. Ferreira[16], F. Fidecaro[18,72], P. Figura[101], I. Fiori[40], M. Fishbach[15], R. P. Fisher[54], R. Fittipaldi[95,166], V. Fiumara[95,167], R. Flaminio[20,28], E. Floden[61], H. Fong[113], J. A. Font[122,168], B. Fornal[169], P. W. F. Forsyth[8], A. Franke[123], S. Frasca[48,96], F. Frasconi[18], C. Frederick[170], J. P. Freed[33], Z. Frei[151], A. Freise[171], R. Frey[58], P. Fritschel[68], V. V. Frolov[6], G. G. Fronzé[22], Y. Fujii[172], Y. Fujikawa[173], M. Fukunaga[35], M. Fukushima[21], P. Fulda[70], M. Fyffe[6], H. A. Gabbard[67], B. U. Gadre[103], J. R. Gair[103], J. Gais[107], S. Galaudage[5], R. Gamba[13], D. Ganapathy[68], A. Ganguly[19], D. Gao[174], S. G. Gaonkar[11], B. Garaventa[83,111], C. García-Núñez[91], C. García-Quirós[142], F. Garufi[4,23], B. Gateley[65], S. Gaudio[33], V. Gayathri[70], G.-G. Ge[174], G. Gemme[83], A. Gennai[18], J. George[85], O. Gerberding[123], L. Gergely[175], P. Gewecke[123], S. Ghonge[105], Abhirup Ghosh[103], Archisman Ghosh[176], Shaon Ghosh[7,162], Shrobana Ghosh[17], B. Giacomazzo[62,63,64], L. Giacoppo[48,96], J. A. Giaime[2,6], K. D. Giardina[6], D. R. Gibson[91], C. Gier[30], M. Giesler[177], P. Giri[18,72], F. Gissi[80], J. Glanzer[2], A. E. Gleckl[38], P. Godwin[146], E. Goetz[178], R. Goetz[70], N. Gohlke[9,10], B. Goncharov[5,29], G. González[2], A. Gopakumar[179], M. Gosselin[40], R. Gouaty[28], D. W. Gould[8], B. Grace[8], A. Grado[4,180], M. Granata[155], V. Granata[94], A. Grant[67], S. Gras[68], P. Grassia[1], C. Gray[65], R. Gray[67], G. Greco[73], A. C. Green[70], R. Green[17], A. M. Gretarsson[33], E. M. Gretarsson[33], D. Griffith[1], W. Griffiths[17], H. L. Griggs[105], G. Grignani[73,74], A. Grimaldi[89,90], S. J. Grimm[29,99], H. Grote[17], S. Grunewald[103], P. Gruning[39], D. Guerra[122], G. M. Guidi[46,47], A. R. Guimaraes[2], G. Guixé[27], H. K. Gulati[78], H.-K. Guo[169], Y. Guo[50], Anchal Gupta[1], Anuradha Gupta[181], P. Gupta[50,112], E. K. Gustafson[1], R. Gustafson[182], F. Guzman[183], S. Ha[184], L. Haegel[34], A. Hagiwara[35,185], S. Haino[134], O. Halim[32,186], E. D. Hall[68], E. Z. Hamilton[158], G. Hammond[67], W.-B. Han[187], M. Haney[158], J. Hanks[65], C. Hanna[146], M. D. Hannam[17], O. Hannuksela[50,112], H. Hansen[65], T. J. Hansen[33], J. Hanson[6], T. Harder[93], T. Hardwick[2], K. Haris[50,112], J. Harms[29,99], G. M. Harry[188], I. W. Harry[153], D. Hartwig[123], K. Hasegawa[35], B. Haskell[79], R. K. Hasskew[6], C.-J. Haster[68], K. Hattori[189], K. Haughian[67], H. Hayakawa[190], K. Hayama[126], F. J. Hayes[67], J. Healy[124], A. Heidmann[100], A. Heidt[9,10], M. C. Heintze[6], J. Heinze[9,10], J. Heinzel[191], H. Heitmann[93], F. Hellman[192], P. Hello[39], A. F. Helmling-Cornell[58], G. Hemming[40], M. Hendry[67], I. S. Heng[67], E. Hennes[50], J. Hennig[193], M. H. Hennig[193], A. G. Hernandez[82], F. Hernandez Vivanco[5], M. Heurs[9,10], S. Hild[50,152], P. Hill[30], Y. Himemoto[194], A. S. Hines[183], Y. Hiranuma[195], N. Hirata[20], E. Hirose[35], W. C. G. Ho[196], S. Hochheim[9,10], D. Hofman[155], J. N. Hohmann[123], D. G. Holcomb[121], N. A. Holland[8], I. J. Hollows[154], Z. J. Holmes[81], K. Holt[6], D. E. Holz[159], Z. Hong[197], P. Hopkins[17], J. Hough[67], S. Hourihane[131], E. J. Howell[84], C. G. Hoy[17], D. Hoyland[14], A. Hreibi[9,10], B-H. Hsieh[35], Y. Hsu[125], G-Z. Huang[197], H-Y. Huang[134], P. Huang[174], Y-C. Huang[132], Y.-J. Huang[134], Y. Huang[68], M. T. Hübner[5], A. D. Huddart[140], B. Hughey[33], D. C. Y. Hui[198], V. Hui[28], S. Husa[142], S. H. Huttner[67], R. Huxford[146], T. Huynh-Dinh[6], S. Ide[199], B. Idzkowski[101], A. Iess[118,119], B. Ikenoue[21], S. Imam[197], K. Inayoshi[200], C. Ingram[81], Y. Inoue[130], K. Ioka[201], M. Isi[68], K. Isleif[123], K. Ito[202], Y. Itoh[203,204], B. R. Iyer[19], K. Izumi[205], V. JaberianHamedan[84], T. Jacqmin[100], S. J. Jadhav[206], S. P. Jadhav[11], A. L. James[17], A. Z. Jan[124], K. Jani[207], J. Janquart[50,112], K. Janssens[93,208], N. N. Janthalur[206], P. Jaranowski[209], D. Jariwala[70], R. Jaume[142], A. C. Jenkins[51], K. Jenner[81], C. Jeon[210], M. Jeunon[61], W. Jia[68], H.-B. Jin[211,212], G. R. Johns[54], A. W. Jones[84], D. I. Jones[213], J. D. Jones[65], P. Jones[14], R. Jones[67], R. J. G. Jonker[50], L. Ju[84], P. Jung[53], K. Jung[184], J. Junker[9,10], V. Juste[160], K. Kaihotsu[202], T. Kajita[214], M. Kakizaki[189], C. V. Kalaghatgi[17,112], V. Kalogera[15], B. Kamai[1], M. Kamiizumi[190], N. Kanda[203,204], S. Kandhasamy[11], G. Kang[215], J. B. Kanner[1], Y. Kao[125], S. J. Kapadia[19], D. P. Kapasi[8], S. Karat[1], C. Karathanasis[216], S. Karki[87], R. Kashyap[146], M. Kasprzack[1], W. Kastaun[9,10], S. Katsanevas[40], E. Katsavounidis[68], W. Katzman[6], T. Kaur[84], K. Kawabe[65], K. Kawaguchi[35], N. Kawai[217], T. Kawasaki[25], F. Kéfélian[93], D. Keitel[142], J. S. Key[218], S. Khadka[71], F. Y. Khalili[88], S. Khan[17], E. A. Khazanov[219], N. Khetan[29,99], M. Khursheed[85], N. Kijbunchoo[8], C. Kim[220], J. C. Kim[221], J. Kim[222], K. Kim[223], W. S. Kim[224], Y.-M. Kim[225], C. Kimball[15], N. Kimura[185], M. Kinley-Hanlon[67], R. Kirchhoff[9,10], J. S. Kissel[65], N. Kita[25], H. Kitazawa[202], L. Kleybolte[123], S. Klimenko[70], A. M. Knee[178], T. D. Knowles[161], E. Knyazev[68], P. Koch[9,10], G. Koekoek[50,152], Y. Kojima[226], K. Kokeyama[227], S. Koley[29], P. Kolitsidou[17], M. Kolstein[216], K. Komori[25,68], V. Kondrashov[1], A. K. H. Kong[228], A. Kontos[229], N. Koper[9,10], M. Korobko[123], K. Kotake[126], M. Kovalam[84], D. B. Kozak[1], C. Kozakai[44], R. Kozu[190], V. Kringel[9,10], N. V. Krishnendu[9,10], A. Królak[230,231], G. Kuehn[9,10], F. Kuei[125], P. Kuijer[50], A. Kumar[206], P. Kumar[177], Rahul Kumar[65], Rakesh Kumar[78], J. Kume[26], K. Kuns[68], C. Kuo[130], H-S. Kuo[197], Y. Kuromiya[202], S. Kuroyanagi[232,233], K. Kusayanagi[217], S. Kuwahara[113], K. Kwak[184], P. Lagabbe[28], D. Laghi[18,72], E. Lalande[234], T. L. Lam[107], A. Lamberts[93,235], M. Landry[65], B. B. Lane[68], R. N. Lang[68], J. Lange[165], B. Lantz[71], I. La Rosa[28], A. Lartaux-Vollard[39], P. D. Lasky[5], M. Laxen[6], A. Lazzarini[1], C. Lazzaro[75,76], P. Leaci[48,96], S. Leavey[9,10], Y. K. Lecoeuche[178], H. K. Lee[236], H. M. Lee[136], H. W. Lee[221], J. Lee[136], K. Lee[237], R. Lee[132], J. Lehmann[9,10], A. Lemaître[238], M. Leonardi[20], N. Leroy[39], N. Letendre[28], C. Levesque[234], Y. Levin[5], J. N. Leviton[182], K. Leyde[34], A. K. Y. Li[1], B. Li[125], J. Li[15], K. L. Li[239], T. G. F. Li[107], X. Li[131], C-Y. Lin[240], F-K. Lin[134], F-L. Lin[197], H. L. Lin[130], L. C.-C. Lin[184], F. Linde[50,241], S. D. Linker[82], J. N. Linley[67], T. B. Littenberg[242], G. C. Liu[128], J. Liu[9,10], K. Liu[125], X. Liu[7], F. Llamas[148], M. Llorens-Monteagudo[122], R. K. L. Lo[1], A. Lockwood[243], L. T. London[68], A. Longo[244,245], D. Lopez[158], M. Lopez Portilla[112], M. Lorenzini[118,119], V. Loriette[246], M. Lormand[6], G. Losurdo[18], T. P. Lott[105], J. D. Lough[9,10], C. O. Lousto[124], G. Lovelace[38], J. F. Lucaccioni[170], H. Lück[9,10], D. Lumaca[118,119], A. P. Lundgren[153], L.-W. Luo[134], J. E. Lynam[54], R. Macas[153], M. MacInnis[68], D. M. Macleod[17], I. A. O. MacMillan[1], A. Macquet[93], I. Magaña Hernandez[7], C. Magazzù[18], R. M. Magee[1], R. Maggiore[14], M. Magnozzi[83,111], S. Mahesh[161], E. Majorana[48,96], C. Makarem[1], I. Maksimovic[246], S. Maliakal[1], A. Malik[85], N. Man[93], V. Mandic[61], V. Mangano[48,96], J. L. Mango[247], G. L. Mansell[65,68], M. Manske[7], M. Mantovani[40], M. Mapelli[75,76], F. Marchesoni[73,248,249], M. Marchio[20], F. Marion[28], Z. Mark[131], S. Márka[43], Z. Márka[43], C. Markakis[12], A. S. Markosyan[71], A. Markowitz[1], E. Maros[1],

A. Marquina[144], S. Marsat[34], F. Martelli[46,47], I. W. Martin[67], R. M. Martin[162], M. Martinez[216], V. A. Martinez[70], V. Martinez[24], K. Martinovic[51], D. V. Martynov[14], E. J. Marx[68], H. Masalehdan[123], K. Mason[68], E. Massera[154], A. Masserot[28], T. J. Massinger[68], M. Masso-Reid[67], S. Mastrogiovanni[34], A. Matas[103], M. Mateu-Lucena[142], F. Matichard[1,68], M. Matiushechkina[9,10], N. Mavalvala[68], J. J. McCann[84], R. McCarthy[65], D. E. McClelland[8], P. K. McClincy[146], S. McCormick[6], L. McCuller[68], G. I. McGhee[67], S. C. McGuire[250], C. McIsaac[153], J. McIver[178], T. McRae[8], S. T. McWilliams[161], D. Meacher[7], M. Mehmet[9,10], A. K. Mehta[103], Q. Meijer[112], A. Melatos[115], D. A. Melchor[38], G. Mendell[65], A. Menendez-Vazquez[216], C. S. Menoni[163], R. A. Mercer[7], L. Mereni[155], K. Merfeld[58], E. L. Merilh[6], J. D. Merritt[58], M. Merzougui[93], S. Meshkov[1,325], C. Messenger[67], C. Messick[165], P. M. Meyers[115], F. Meylahn[9,10], A. Mhaske[11], A. Miani[89,90], H. Miao[14], I. Michaloliakos[70], C. Michel[155], Y. Michimura[25], H. Middleton[115], L. Milano[23], A. L. Miller[49], A. Miller[82], B. Miller[50,86], M. Millhouse[115], J. C. Mills[17], E. Milotti[32,186], O. Minazzoli[93,251], Y. Minenkov[119], N. Mio[252], Ll. M. Mir[216], M. Miravet-Tenés[122], C. Mishra[253], T. Mishra[70], T. Mistry[154], S. Mitra[11], V. P. Mitrofanov[88], G. Mitselmakher[70], R. Mittleman[68], O. Miyakawa[190], A. Miyamoto[203], Y. Miyazaki[25], K. Miyo[190], S. Miyoki[190], Geoffrey Mo[68], L. M. Modafferi[142], E. Moguel[170], K. Mogushi[87], S. R. P. Mohapatra[68], S. R. Mohite[7], I. Molina[38], M. Molina-Ruiz[192], M. Mondin[82], M. Montani[46,47], C. J. Moore[14], J. Moragues[142], D. Moraru[65], F. Morawski[79], A. More[11], C. Moreno[33], G. Moreno[65], Y. Mori[202], S. Morisaki[7], Y. Moriwaki[189], B. Mours[160], C. M. Mow-Lowry[14,171], S. Mozzon[153], F. Muciaccia[48,96], Arunava Mukherjee[254], D. Mukherjee[146], Soma Mukherjee[148], Subroto Mukherjee[78], Suvodip Mukherjee[86], N. Mukund[9,10], A. Mullavey[6], J. Munch[81], E. A. Muñiz[59], P. G. Murray[67], R. Musenich[83,111], S. Muusse[81], S. L. Nadji[9,10], K. Nagano[205], S. Nagano[255], A. Nagar[22,256], K. Nakamura[20], H. Nakano[257], M. Nakano[35], R. Nakashima[217], Y. Nakayama[202], V. Napolano[40], I. Nardecchia[118,119], T. Narikawa[35], L. Naticchioni[48], B. Nayak[82], R. K. Nayak[258], R. Negishi[195], B. F. Neil[84], J. Neilson[80,95], G. Nelemans[259], T. J. N. Nelson[6], M. Nery[9,10], P. Neubauer[170], A. Neunzert[218], K. Y. Ng[68], S. W. S. Ng[81], C. Nguyen[34], P. Nguyen[58], T. Nguyen[68], L. Nguyen Quynh[260], W.-T. Ni[132,174,211], S. A. Nichols[2], A. Nishizawa[26], S. Nissanke[50,86], E. Nitoglia[135], F. Nocera[40], M. Norman[17], C. North[17], S. Nozaki[189], L. K. Nuttall[153], J. Oberling[65], B. D. O'Brien[70], Y. Obuchi[21], J. O'Dell[140], E. Oelker[67], W. Ogaki[35], G. Oganesyan[29,99], J. J. Oh[224], K. Oh[198], S. H. Oh[224], M. Ohashi[190], N. Ohishi[44], M. Ohkawa[173], F. Ohme[9,10], H. Ohta[113], M. A. Okada[16], Y. Okutani[199], K. Okutomi[190], C. Olivetto[40], K. Oohara[195], C. Ooi[25], R. Oram[6], B. O'Reilly[6], R. G. Ormiston[61], N. D. Ormsby[54], L. F. Ortega[70], R. O'Shaughnessy[124], E. O'Shea[177], S. Oshino[190], S. Ossokine[103], C. Osthelder[1], S. Otabe[217], D. J. Ottaway[81], H. Overmier[6], A. E. Pace[146], G. Pagano[18,72], M. A. Page[84], G. Pagliaroli[29,99], A. Pai[98], S. A. Pai[85], J. R. Palamos[58], O. Palashov[219], C. Palomba[48], H. Pan[125], K. Pan[132,228], P. K. Panda[206], H. Pang[130], P. T. H. Pang[50,112], C. Pankow[15], F. Pannarale[48,96], B. C. Pant[85], F. H. Panther[84], F. Paoletti[18], A. Paoli[40], A. Paolone[48,261], A. Parisi[128], H. Park[7], J. Park[262], W. Parker[6,250], D. Pascucci[50], A. Pasqualetti[40], R. Passaquieti[18,72], D. Passuello[18], M. Patel[54], M. Pathak[81], B. Patricelli[18,40], A. S. Patron[2], S. Patrone[48,96], S. Paul[58], E. Payne[5], M. Pedraza[1], M. Pegoraro[76], A. Pele[6], F. E. Peña Arellano[190], S. Penn[263], A. Perego[89,90], A. Pereira[24], T. Pereira[264], C. J. Perez[65], C. Périgois[28], C. C. Perkins[70], A. Perreca[89,90], S. Perriès[135], J. Petermann[123], D. Petterson[1], H. P. Pfeiffer[103], K. A. Pham[61], K. S. Phukon[50,241], O. J. Piccinni[48], M. Pichot[93], M. Piendibene[18,72], F. Piergiovanni[46,47], L. Pierini[48,96], V. Pierro[80,95], G. Pillant[40], M. Pillas[39], F. Pilo[18], L. Pinard[155], I. M. Pinto[80,95,265], M. Pinto[40], K. Piotrzkowski[49], M. Pirello[65], M. D. Pitkin[266], E. Placidi[48,96], L. Planas[142], W. Plastino[244,245], C. Pluchar[139], R. Poggiani[18,72], E. Polini[28], D. Y. T. Pong[107], S. Ponrathnam[11], P. Popolizio[40], E. K. Porter[34], R. Poulton[40], J. Powell[55], M. Pracchia[28], T. Pradier[160], A. K. Prajapati[78], K. Prasai[71], R. Prasanna[206], G. Pratten[14], M. Principe[80,95,265], G. A. Prodi[90,267], L. Prokhorov[14], P. Prosposito[118,119], L. Prudenzi[103], A. Puecher[50,112], M. Punturo[73], F. Puosi[18,72], P. Puppo[48], M. Pürrer[103], H. Qi[17], V. Quetschke[148], R. Quitzow-James[87], F. J. Raab[65], G. Raaijmakers[50,86], H. Radkins[65], N. Radulesco[93], P. Raffai[151], S. X. Rail[234], S. Raja[85], C. Rajan[85], K. E. Ramirez[6], T. D. Ramirez[38], A. Ramos-Buades[103], J. Rana[146], P. Rapagnani[48,96], U. D. Rapol[268], A. Ray[7], V. Raymond[17], N. Raza[178], M. Razzano[18,72], J. Read[38], L. A. Rees[188], T. Regimbau[28], L. Rei[83], S. Reid[30], S. W. Reid[54], D. H. Reitze[1,70], P. Relton[17], A. Renzini[1], P. Rettegno[22,269], M. Rezac[38], F. Ricci[48,96], D. Richards[140], J. W. Richardson[1], L. Richardson[183], G. Riemenschneider[22,269], K. Riles[182], S. Rinaldi[18,72], K. Rink[178], M. Rizzo[15], N. A. Robertson[1,67], R. Robie[1], F. Robinet[39], A. Rocchi[119], S. Rodriguez[38], L. Rolland[28], J. G. Rollins[1], M. Romanelli[97], R. Romano[3,4], C. L. Romel[65], A. Romero-Rodríguez[216], I. M. Romero-Shaw[5], J. H. Romie[6], S. Ronchini[29,99], L. Rosa[4,23], C. A. Rose[7], D. Rosińska[101], M. P. Ross[243], S. Rowan[67], S. J. Rowlinson[14], S. Roy[112], Santosh Roy[11], Soumen Roy[270], D. Rozza[116,117], P. Ruggi[40], K. Ryan[65], S. Sachdev[146], T. Sadecki[65], J. Sadiq[106], N. Sago[271], S. Saito[21], Y. Saito[190], K. Sakai[272], Y. Sakai[195], M. Sakellariadou[51], Y. Sakuno[126], O. S. Salafia[62,63,64], L. Salconi[40], M. Saleem[61], F. Salemi[89,90], A. Samajdar[50,112], E. J. Sanchez[1], J. H. Sanchez[38], L. E. Sanchez[1], N. Sanchis-Gual[273], J. R. Sanders[274], A. Sanuy[27], T. R. Saravanan[11], N. Sarin[5], B. Sassolas[155], H. Satari[84], S. Sato[275], T. Sato[173], O. Sauter[70], R. L. Savage[65], T. Sawada[203], D. Sawant[98], H. L. Sawant[11], S. Sayah[155], D. Schaetzl[1], M. Scheel[131], J. Scheuer[15], M. Schiworski[81], P. Schmidt[14], S. Schmidt[112], R. Schnabel[123], M. Schneewind[9,10], R. M. S. Schofield[58], A. Schönbeck[123], B. W. Schulte[9,10], B. F. Schutz[9,10,17], E. Schwartz[17], J. Scott[67], S. M. Scott[8], M. Seglar-Arroyo[28], T. Sekiguchi[26], Y. Sekiguchi[276], D. Sellers[6], A. S. Sengupta[270], D. Sentenac[40], E. G. Seo[107], V. Sequino[4,23], A. Sergeev[219], Y. Setyawati[112], T. Shaffer[65], M. S. Shahriar[15], B. Shams[169], L. Shao[200], A. Sharma[29,99], P. Sharma[85], P. Shawhan[102], N. S. Shcheblanov[238], S. Shibagaki[126], M. Shikauchi[113], R. Shimizu[21], T. Shimoda[25], K. Shimode[190], H. Shinkai[277], T. Shishido[45], A. Shoda[20], D. H. Shoemaker[68], D. M. Shoemaker[165], S. ShyamSundar[85], M. Sieniawska[101], D. Sigg[65], L. P. Singer[110], D. Singh[146], N. Singh[101], A. Singha[50,152], A. M. Sintes[142], V. Sipala[116,117], V. Skliris[17], B. J. J. Slagmolen[8], T. J. Slaven-Blair[84], J. Smetana[14], J. R. Smith[38], R. J. E. Smith[5], J. Soldateschi[47,278,279], S. N. Somala[280], K. Somiya[217], E. J. Son[224], K. Soni[11], S. Soni[2], V. Sordini[135], F. Sorrentino[83], N. Sorrentino[18,72], H. Sotani[281],

R. Soulard[93], T. Souradeep[11,268], E. Sowell[145], V. Spagnuolo[50,152], A. P. Spencer[67], M. Spera[75,76], R. Srinivasan[93], A. K. Srivastava[78], V. Srivastava[59], K. Staats[15], C. Stachie[93], D. A. Steer[34], J. Steinlechner[50,152], S. Steinlechner[50,152], D. J. Stops[14], M. Stover[170], K. A. Strain[67], L. C. Strang[115], G. Stratta[47,282], A. Strunk[65], R. Sturani[264], A. L. Stuver[121], S. Sudhagar[11], V. Sudhir[68], R. Sugimoto[205,283], H. G. Suh[7], T. Z. Summerscales[284], H. Sun[84], L. Sun[8], S. Sunil[78], A. Sur[79], J. Suresh[35,113], P. J. Sutton[17], Takamasa Suzuki[173], Toshikazu Suzuki[35], B. L. Swinkels[50], M. J. Szczepańczyk[70], P. Szewczyk[101], M. Tacca[50], H. Tagoshi[35], S. C. Tait[67], H. Takahashi[285], R. Takahashi[20], A. Takamori[37], S. Takano[25], H. Takeda[25], M. Takeda[203], C. J. Talbot[30], C. Talbot[1], H. Tanaka[286], Kazuyuki Tanaka[203], Kenta Tanaka[286], Taiki Tanaka[35], Takahiro Tanaka[271], A. J. Tanasijczuk[49], S. Tanioka[20,45], D. B. Tanner[70], D. Tao[1], L. Tao[70], E. N. Tapia San Martín[20,50], C. Taranto[118], J. D. Tasson[191], S. Telada[287], R. Tenorio[142], J. E. Terhune[121], L. Terkowski[123], M. P. Thirugnanasambandam[11], M. Thomas[6], P. Thomas[65], J. E. Thompson[17], S. R. Thondapu[85], K. A. Thorne[6], E. Thrane[5], Shubhanshu Tiwari[158], Srishti Tiwari[11], V. Tiwari[17], A. M. Toivonen[61], K. Toland[67], A. E. Tolley[153], T. Tomaru[20], Y. Tomigami[203], T. Tomura[190], M. Tonelli[18,72], A. Torres-Forné[122], C. I. Torrie[1], I. Tosta e Melo[116,117], D. Töyrä[8], A. Trapananti[73,248], F. Travasso[73,248], G. Traylor[6], M. Trevor[102], M. C. Tringali[40], A. Tripathee[182], L. Troiano[95,288], A. Trovato[34], L. Trozzo[4,190], R. J. Trudeau[1], D. S. Tsai[125], D. Tsai[125], K. W. Tsang[50,112,289], T. Tsang[290], J-S. Tsao[197], M. Tse[68], R. Tso[131], K. Tsubono[25], S. Tsuchida[203], L. Tsukada[113], D. Tsuna[113], T. Tsutsui[113], T. Tsuzuki[21], K. Turbang[208,291], M. Turconi[93], D. Tuyenbayev[203], A. S. Ubhi[14], N. Uchikata[35], T. Uchiyama[190], R. P. Udall[1], A. Ueda[185], T. Uehara[292,293], K. Ueno[113], G. Ueshima[294], C. S. Unnikrishnan[179], F. Uraguchi[21], A. L. Urban[2], T. Ushiba[190], A. Utina[50,152], H. Vahlbruch[9,10], G. Vajente[1], A. Vajpeyi[5], G. Valdes[183], M. Valentini[89,90], V. Valsan[7], N. van Bakel[50], M. van Beuzekom[50], J. F. J. van den Brand[50,152,295], C. Van Den Broeck[50,112], D. C. Vander-Hyde[59], L. van der Schaaf[50], J. V. van Heijningen[49], J. Vanosky[1], M. H. P. M. van Putten[296], N. van Remortel[208], M. Vardaro[50,241], A. F. Vargas[115], V. Varma[177], M. Vasúth[69], A. Vecchio[14], G. Vedovato[76], J. Veitch[67], P. J. Veitch[81], J. Venneberg[9,10], G. Venugopalan[1], D. Verkindt[28], P. Verma[231], Y. Verma[85], D. Veske[43], F. Vetrano[46], A. Viceré[46,47], S. Vidyant[59], A. D. Viets[247], A. Vijaykumar[19], V. Villa-Ortega[106], J.-Y. Vinet[93], A. Virtuoso[32,186], S. Vitale[68], T. Vo[59], H. Vocca[73,74], E. R. G. von Reis[65], J. S. A. von Wrangel[9,10], C. Vorvick[65], S. P. Vyatchanin[88], L. E. Wade[170], M. Wade[170], K. J. Wagner[124], R. C. Walet[50], M. Walker[54], G. S. Wallace[30], L. Wallace[1], S. Walsh[7], J. Wang[174], J. Z. Wang[182], W. H. Wang[148], R. L. Ward[8], J. Warner[65], M. Was[28], T. Washimi[20], N. Y. Washington[1], J. Watchi[143], B. Weaver[65], S. A. Webster[67], M. Weinert[9,10], A. J. Weinstein[1], R. Weiss[68], C. M. Weller[243], F. Wellmann[9,10], L. Wen[84], P. Weßels[9,10], K. Wette[8], J. T. Whelan[124], D. D. White[38], B. F. Whiting[70], C. Whittle[68], D. Wilken[9,10], D. Williams[67], M. J. Williams[67], A. R. Williamson[153], J. L. Willis[1], B. Willke[9,10], D. J. Wilson[139], W. Winkler[9,10], C. C. Wipf[1], T. Wlodarczyk[103], G. Woan[67], J. Woehler[9,10], J. K. Wofford[124], I. C. F. Wong[107], C. Wu[132], D. S. Wu[9,10], H. Wu[132], S. Wu[132], D. M. Wysocki[7], L. Xiao[1], W-R. Xu[197], T. Yamada[286], H. Yamamoto[1], Kazuhiro Yamamoto[189], Kohei Yamamoto[286], T. Yamamoto[190], K. Yamashita[202], R. Yamazaki[199], F. W. Yang[169], L. Yang[163], Y. Yang[297], Yang Yang[70], Z. Yang[61], M. J. Yap[8], D. W. Yeeles[17], A. B. Yelikar[124], M. Ying[125], K. Yokogawa[202], J. Yokoyama[25,26], T. Yokozawa[190], J. Yoo[177], T. Yoshioka[202], Hang Yu[131], Haocun Yu[68], H. Yuzurihara[35], A. Zadrożny[231], M. Zanolin[33], S. Zeidler[298], T. Zelenova[40], J.-P. Zendri[76], M. Zevin[159], M. Zhan[174], H. Zhang[197], J. Zhang[84], L. Zhang[1], T. Zhang[14], Y. Zhang[183], C. Zhao[84], G. Zhao[143], Y. Zhao[20], Yue Zhao[169], R. Zhou[192], Z. Zhou[15], X. J. Zhu[5], Z.-H. Zhu[114], M. E. Zucker[1,68], J. Zweizig[1]

The LIGO Scientific Collaboration, the Virgo Collaboration, and the KAGRA Collaboration,

D. Antonopoulou[299], Z. Arzoumanian[300], A. Basu[299], S. Bogdanov[301], I. Cognard[302,303], K. Crowter[304], T. Enoto[305], C. M. Espinoza[306,307], C. M. L. Flynn[55], E. Fonseca[308,309], D. C. Good[310,311], L. Guillemot[302,303], S. Guillot[312,313], A. K. Harding[314], M. J. Keith[299], L. Kuiper[315], M. E. Lower[316,317], A. G. Lyne[299], J. W. McKee[318], B. W. Meyers[304], C. Ng[319], J. L. Palfreyman[320], R. M. Shannon[316,321], B. Shaw[299], I. H. Stairs[304], B. W. Stappers[299], C. M. Tan[322,323], G. Theureau[302,303,324], and P. Weltevrede[299]

[1] LIGO Laboratory, California Institute of Technology, Pasadena, CA 91125, USA; lvc.publications@ligo.org
[2] Louisiana State University, Baton Rouge, LA 70803, USA
[3] Dipartimento di Farmacia, Università di Salerno, I-84084 Fisciano, Salerno, Italy
[4] INFN, Sezione di Napoli, Complesso Universitario di Monte S. Angelo, I-80126 Napoli, Italy
[5] OzGrav, School of Physics & Astronomy, Monash University, Clayton 3800, Victoria, Australia
[6] LIGO Livingston Observatory, Livingston, LA 70754, USA
[7] University of Wisconsin-Milwaukee, Milwaukee, WI 53201, USA
[8] OzGrav, Australian National University, Canberra, Australian Capital Territory 0200, Australia
[9] Max Planck Institute for Gravitational Physics (Albert Einstein Institute), D-30167 Hannover, Germany
[10] Leibniz Universität Hannover, D-30167 Hannover, Germany
[11] Inter-University Centre for Astronomy and Astrophysics, Pune 411007, India
[12] University of Cambridge, Cambridge CB2 1TN, UK
[13] Theoretisch-Physikalisches Institut, Friedrich-Schiller-Universität Jena, D-07743 Jena, Germany
[14] University of Birmingham, Birmingham B15 2TT, UK
[15] Center for Interdisciplinary Exploration & Research in Astrophysics (CIERA), Northwestern University, Evanston, IL 60208, USA
[16] Instituto Nacional de Pesquisas Espaciais, 12227-010 São José dos Campos, São Paulo, Brazil
[17] Gravity Exploration Institute, Cardiff University, Cardiff CF24 3AA, UK
[18] INFN, Sezione di Pisa, I-56127 Pisa, Italy
[19] International Centre for Theoretical Sciences, Tata Institute of Fundamental Research, Bengaluru 560089, India
[20] Gravitational Wave Science Project, National Astronomical Observatory of Japan (NAOJ), Mitaka City, Tokyo 181-8588, Japan
[21] Advanced Technology Center, National Astronomical Observatory of Japan (NAOJ), Mitaka City, Tokyo 181-8588, Japan
[22] INFN Sezione di Torino, I-10125 Torino, Italy
[23] Università di Napoli "Federico II," Complesso Universitario di Monte S. Angelo, I-80126 Napoli, Italy

[24] Université de Lyon, Université Claude Bernard Lyon 1, CNRS, Institut Lumière Matière, F-69622 Villeurbanne, France
[25] Department of Physics, The University of Tokyo, Bunkyo-ku, Tokyo 113-0033, Japan
[26] Research Center for the Early Universe (RESCEU), The University of Tokyo, Bunkyo-ku, Tokyo 113-0033, Japan
[27] Institut de Ciències del Cosmos (ICCUB), Universitat de Barcelona, C/ Martí i Franquès 1, Barcelona, E-08028, Spain
[28] Laboratoire d'Annecy de Physique des Particules (LAPP), Univ. Grenoble Alpes, Université Savoie Mont Blanc, CNRS/IN2P3, F-74941 Annecy, France
[29] Gran Sasso Science Institute (GSSI), I-67100 L'Aquila, Italy
[30] SUPA, University of Strathclyde, Glasgow G1 1XQ, UK
[31] Dipartimento di Scienze Matematiche, Informatiche e Fisiche, Università di Udine, I-33100 Udine, Italy
[32] INFN, Sezione di Trieste, I-34127 Trieste, Italy
[33] Embry-Riddle Aeronautical University, Prescott, AZ 86301, USA
[34] Université de Paris, CNRS, Astroparticule et Cosmologie, F-75006 Paris, France
[35] Institute for Cosmic Ray Research (ICRR), KAGRA Observatory, The University of Tokyo, Kashiwa City, Chiba 277-8582, Japan
[36] Accelerator Laboratory, High Energy Accelerator Research Organization (KEK), Tsukuba City, Ibaraki 305-0801, Japan
[37] Earthquake Research Institute, The University of Tokyo, Bunkyo-ku, Tokyo 113-0032, Japan
[38] California State University Fullerton, Fullerton, CA 92831, USA
[39] Université Paris-Saclay, CNRS/IN2P3, IJCLab, F-91405 Orsay, France
[40] European Gravitational Observatory (EGO), I-56021 Cascina, Pisa, Italy
[41] Chennai Mathematical Institute, Chennai 603103, India
[42] Department of Mathematics and Physics, Gravitational Wave Science Project, Hirosaki University, Hirosaki City, Aomori 036-8561, Japan
[43] Columbia University, New York, NY 10027, USA
[44] Kamioka Branch, National Astronomical Observatory of Japan (NAOJ), Kamioka-cho, Hida City, Gifu 506-1205, Japan
[45] The Graduate University for Advanced Studies (SOKENDAI), Mitaka City, Tokyo 181-8588, Japan
[46] Università degli Studi di Urbino "Carlo Bo," I-61029 Urbino, Italy
[47] INFN, Sezione di Firenze, I-50019 Sesto Fiorentino, Firenze, Italy
[48] INFN, Sezione di Roma, I-00185 Roma, Italy
[49] Université catholique de Louvain, B-1348 Louvain-la-Neuve, Belgium
[50] Nikhef, Science Park 105, 1098 XG Amsterdam, Netherlands
[51] King's College London, University of London, London WC2R 2LS, UK
[52] Korea Institute of Science and Technology Information (KISTI), Yuseong-gu, Daejeon 34141, Republic of Korea
[53] National Institute for Mathematical Sciences, Yuseong-gu, Daejeon 34047, Republic of Korea
[54] Christopher Newport University, Newport News, VA 23606, USA
[55] OzGrav, Swinburne University of Technology, Hawthorn VIC 3122, Australia
[56] International College, Osaka University, Toyonaka City, Osaka 560-0043, Japan
[57] School of High Energy Accelerator Science, The Graduate University for Advanced Studies (SOKENDAI), Tsukuba City, Ibaraki 305-0801, Japan
[58] University of Oregon, Eugene, OR 97403, USA
[59] Syracuse University, Syracuse, NY 13244, USA
[60] Université de Liège, B-4000 Liège, Belgium
[61] University of Minnesota, Minneapolis, MN 55455, USA
[62] Università degli Studi di Milano-Bicocca, I-20126 Milano, Italy
[63] INFN, Sezione di Milano-Bicocca, I-20126 Milano, Italy
[64] INAF, Osservatorio Astronomico di Brera sede di Merate, I-23807 Merate, Lecco, Italy
[65] LIGO Hanford Observatory, Richland, WA 99352, USA
[66] Dipartimento di Medicina, Chirurgia e Odontoiatria "Scuola Medica Salernitana,"Università di Salerno, I-84081 Baronissi, Salerno, Italy
[67] SUPA, University of Glasgow, Glasgow G12 8QQ, UK
[68] LIGO Laboratory, Massachusetts Institute of Technology, Cambridge, MA 02139, USA
[69] Wigner RCP, RMKI, H-1121 Budapest, Konkoly Thege Miklós út 29-33, Hungary
[70] University of Florida, Gainesville, FL 32611, USA
[71] Stanford University, Stanford, CA 94305, USA
[72] Università di Pisa, I-56127 Pisa, Italy
[73] INFN, Sezione di Perugia, I-06123 Perugia, Italy
[74] Università di Perugia, I-06123 Perugia, Italy
[75] Università di Padova, Dipartimento di Fisica e Astronomia, I-35131 Padova, Italy
[76] INFN, Sezione di Padova, I-35131 Padova, Italy
[77] Montana State University, Bozeman, MT 59717, USA
[78] Institute for Plasma Research, Bhat, Gandhinagar 382428, India
[79] Nicolaus Copernicus Astronomical Center, Polish Academy of Sciences, 00-716, Warsaw, Poland
[80] Dipartimento di Ingegneria, Università del Sannio, I-82100 Benevento, Italy
[81] OzGrav, University of Adelaide, Adelaide, South Australia 5005, Australia
[82] California State University, Los Angeles, 5151 State University Dr, Los Angeles, CA 90032, USA
[83] INFN, Sezione di Genova, I-16146 Genova, Italy
[84] OzGrav, University of Western Australia, Crawley, Western Australia 6009, Australia
[85] RRCAT, Indore, Madhya Pradesh 452013, India
[86] GRAPPA, Anton Pannekoek Institute for Astronomy and Institute for High-Energy Physics, University of Amsterdam, Science Park 904, 1098 XH Amsterdam, Netherlands
[87] Missouri University of Science and Technology, Rolla, MO 65409, USA
[88] Faculty of Physics, Lomonosov Moscow State University, Moscow 119991, Russia
[89] Università di Trento, Dipartimento di Fisica, I-38123 Povo, Trento, Italy
[90] INFN, Trento Institute for Fundamental Physics and Applications, I-38123 Povo, Trento, Italy
[91] SUPA, University of the West of Scotland, Paisley PA1 2BE, UK
[92] Bar-Ilan University, Ramat Gan, 5290002, Israel
[93] Artemis, Université Côte d'Azur, Observatoire de la Côte d'Azur, CNRS, F-06304 Nice, France
[94] Dipartimento di Fisica "E.R. Caianiello,"Università di Salerno, I-84084 Fisciano, Salerno, Italy
[95] INFN, Sezione di Napoli, Gruppo Collegato di Salerno, Complesso Universitario di Monte S. Angelo, I-80126 Napoli, Italy
[96] Università di Roma "La Sapienza", I-00185 Roma, Italy
[97] Univ Rennes, CNRS, Institut FOTON—UMR6082, F-3500 Rennes, France
[98] Indian Institute of Technology Bombay, Powai, Mumbai 400 076, India

[99] INFN, Laboratori Nazionali del Gran Sasso, I-67100 Assergi, Italy
[100] Laboratoire Kastler Brossel, Sorbonne Université, CNRS, ENS-Université PSL, Collège de France, F-75005 Paris, France
[101] Astronomical Observatory Warsaw University, 00-478 Warsaw, Poland
[102] University of Maryland, College Park, MD 20742, USA
[103] Max Planck Institute for Gravitational Physics (Albert Einstein Institute), D-14476 Potsdam, Germany
[104] L2IT, Laboratoire des 2 Infinis—Toulouse, Université de Toulouse, CNRS/IN2P3, UPS, F-31062 Toulouse Cedex 9, France
[105] School of Physics, Georgia Institute of Technology, Atlanta, GA 30332, USA
[106] IGFAE, Campus Sur, Universidade de Santiago de Compostela, E-15782 Spain
[107] The Chinese University of Hong Kong, Shatin, NT, Hong Kong
[108] Stony Brook University, Stony Brook, NY 11794, USA
[109] Center for Computational Astrophysics, Flatiron Institute, New York, NY 10010, USA
[110] NASA Goddard Space Flight Center, Greenbelt, MD 20771, USA
[111] Dipartimento di Fisica, Università degli Studi di Genova, I-16146 Genova, Italy
[112] Institute for Gravitational and Subatomic Physics (GRASP), Utrecht University, Princetonplein 1, 3584 CC Utrecht, Netherlands
[113] RESCEU, University of Tokyo, Tokyo, 113-0033, Japan
[114] Department of Astronomy, Beijing Normal University, Beijing 100875, People's Republic of China
[115] OzGrav, University of Melbourne, Parkville, Victoria 3010, Australia
[116] Università degli Studi di Sassari, I-07100 Sassari, Italy
[117] INFN, Laboratori Nazionali del Sud, I-95125 Catania, Italy
[118] Università di Roma Tor Vergata, I-00133 Roma, Italy
[119] INFN, Sezione di Roma Tor Vergata, I-00133 Roma, Italy
[120] University of Sannio at Benevento, I-82100 Benevento, Italy and INFN, Sezione di Napoli, I-80100 Napoli, Italy
[121] Villanova University, 800 Lancaster Ave, Villanova, PA 19085, USA
[122] Departamento de Astronomía y Astrofísica, Universitat de València, E-46100 Burjassot, València, Spain
[123] Universität Hamburg, D-22761 Hamburg, Germany
[124] Rochester Institute of Technology, Rochester, NY 14623, USA
[125] National Tsing Hua University, Hsinchu City, 30013 Taiwan, People's Republic of China
[126] Department of Applied Physics, Fukuoka University, Jonan, Fukuoka City, Fukuoka 814-0180, Japan
[127] OzGrav, Charles Sturt University, Wagga Wagga, New South Wales 2678, Australia
[128] Department of Physics, Tamkang University, Danshui Dist., New Taipei City 25137, Taiwan
[129] Department of Physics and Institute of Astronomy, National Tsing Hua University, Hsinchu 30013, Taiwan
[130] Department of Physics, Center for High Energy and High Field Physics, National Central University, Zhongli District, Taoyuan City 32001, Taiwan
[131] CaRT, California Institute of Technology, Pasadena, CA 91125, USA
[132] Department of Physics, National Tsing Hua University, Hsinchu 30013, Taiwan
[133] Dipartimento di Ingegneria Industriale (DIIN), Università di Salerno, I-84084 Fisciano, Salerno, Italy
[134] Institute of Physics, Academia Sinica, Nankang, Taipei 11529, Taiwan
[135] Université Lyon, Université Claude Bernard Lyon 1, CNRS, IP2I Lyon/IN2P3, UMR 5822, F-69622 Villeurbanne, France
[136] Seoul National University, Seoul 08826, Republic of Korea
[137] Pusan National University, Busan 46241, Republic of Korea
[138] INAF, Osservatorio Astronomico di Padova, I-35122 Padova, Italy
[139] University of Arizona, Tucson, AZ 85721, USA
[140] Rutherford Appleton Laboratory, Didcot OX11 0DE, UK
[141] Université libre de Bruxelles, Avenue Franklin Roosevelt 50, B-1050 Bruxelles, Belgium
[142] Universitat de les Illes Balears, IAC3—IEEC, E-07122 Palma de Mallorca, Spain
[143] Université Libre de Bruxelles, Brussels B-1050, Belgium
[144] Departamento de Matemáticas, Universitat de València, E-46100 Burjassot, València, Spain
[145] Texas Tech University, Lubbock, TX 79409, USA
[146] The Pennsylvania State University, University Park, PA 16802, USA
[147] University of Rhode Island, Kingston, RI 02881, USA
[148] The University of Texas Rio Grande Valley, Brownsville, TX 78520, USA
[149] Bellevue College, Bellevue, WA 98007, USA
[150] Scuola Normale Superiore, Piazza dei Cavalieri, 7, I-56126 Pisa, Italy
[151] MTA-ELTE Astrophysics Research Group, Institute of Physics, Eötvös University, Budapest 1117, Hungary
[152] Maastricht University, P.O. Box 616, 6200 MD Maastricht, Netherlands
[153] University of Portsmouth, Portsmouth, PO1 3FX, UK
[154] The University of Sheffield, Sheffield S10 2TN, UK
[155] Université Lyon, Université Claude Bernard Lyon 1, CNRS, Laboratoire des Matériaux Avancés (LMA), IP2I Lyon/IN2P3, UMR 5822, F-69622 Villeurbanne, France
[156] Dipartimento di Scienze Matematiche, Fisiche e Informatiche, Università di Parma, I-43124 Parma, Italy
[157] INFN, Sezione di Milano Bicocca, Gruppo Collegato di Parma, I-43124 Parma, Italy
[158] Physik-Institut, University of Zurich, Winterthurerstrasse 190, 8057 Zurich, Switzerland
[159] University of Chicago, Chicago, IL 60637, USA
[160] Université de Strasbourg, CNRS, IPHC UMR 7178, F-67000 Strasbourg, France
[161] West Virginia University, Morgantown, WV 26506, USA
[162] Montclair State University, Montclair, NJ 07043, USA
[163] Colorado State University, Fort Collins, CO 80523, USA
[164] Institute for Nuclear Research, Hungarian Academy of Sciences, Bem t'er 18/c, H-4026 Debrecen, Hungary
[165] Department of Physics, University of Texas, Austin, TX 78712, USA
[166] CNR-SPIN, c/o Università di Salerno, I-84084 Fisciano, Salerno, Italy
[167] Scuola di Ingegneria, Università della Basilicata, I-85100 Potenza, Italy
[168] Observatori Astronòmic, Universitat de València, E-46980 Paterna, València, Spain
[169] The University of Utah, Salt Lake City, UT 84112, USA
[170] Kenyon College, Gambier, OH 43022, USA
[171] Vrije Universiteit Amsterdam, 1081 HV, Amsterdam, Netherlands
[172] Department of Astronomy, The University of Tokyo, Mitaka City, Tokyo 181-8588, Japan
[173] Faculty of Engineering, Niigata University, Nishi-ku, Niigata City, Niigata 950-2181, Japan

[174] State Key Laboratory of Magnetic Resonance and Atomic and Molecular Physics, Innovation Academy for Precision Measurement Science and Technology (APM), Chinese Academy of Sciences, Xiao Hong Shan, Wuhan 430071, People's Republic of China
[175] University of Szeged, Dóm tér 9, Szeged 6720, Hungary
[176] Universiteit Gent, B-9000 Gent, Belgium
[177] Cornell University, Ithaca, NY 14850, USA
[178] University of British Columbia, Vancouver, BC V6T 1Z4, Canada
[179] Tata Institute of Fundamental Research, Mumbai 400005, India
[180] INAF, Osservatorio Astronomico di Capodimonte, I-80131 Napoli, Italy
[181] The University of Mississippi, University, MS 38677, USA
[182] University of Michigan, Ann Arbor, MI 48109, USA
[183] Texas A&M University, College Station, TX 77843, USA
[184] Department of Physics, Ulsan National Institute of Science and Technology (UNIST), Ulju-gun, Ulsan 44919, Republic of Korea
[185] Applied Research Laboratory, High Energy Accelerator Research Organization (KEK), Tsukuba City, Ibaraki 305-0801, Japan
[186] Dipartimento di Fisica, Università di Trieste, I-34127 Trieste, Italy
[187] Shanghai Astronomical Observatory, Chinese Academy of Sciences, Shanghai 200030, People's Republic of China
[188] American University, Washington, DC 20016, USA
[189] Faculty of Science, University of Toyama, Toyama City, Toyama 930-8555, Japan
[190] Institute for Cosmic Ray Research (ICRR), KAGRA Observatory, The University of Tokyo, Kamioka-cho, Hida City, Gifu 506-1205, Japan
[191] Carleton College, Northfield, MN 55057, USA
[192] University of California, Berkeley, CA 94720, USA
[193] Maastricht University, 6200 MD, Maastricht, Netherlands
[194] College of Industrial Technology, Nihon University, Narashino City, Chiba 275-8575, Japan
[195] Graduate School of Science and Technology, Niigata University, Nishi-ku, Niigata City, Niigata 950-2181, Japan
[196] Department of Physics and Astronomy, Haverford College, 370 Lancaster Avenue, Haverford, PA 19041, USA
[197] Department of Physics, National Taiwan Normal University, sec. 4, Taipei 116, Taiwan
[198] Astronomy & Space Science, Chungnam National University, Yuseong-gu, Daejeon 34134, Republic of Korea
[199] Department of Physics and Mathematics, Aoyama Gakuin University, Sagamihara City, Kanagawa 252-5258, Japan
[200] Kavli Institute for Astronomy and Astrophysics, Peking University, Haidian District, Beijing 100871, People's Republic of China
[201] Yukawa Institute for Theoretical Physics (YITP), Kyoto University, Sakyou-ku, Kyoto City, Kyoto 606-8502, Japan
[202] Graduate School of Science and Engineering, University of Toyama, Toyama City, Toyama 930-8555, Japan
[203] Department of Physics, Graduate School of Science, Osaka City University, Sumiyoshi-ku, Osaka City, Osaka 558-8585, Japan
[204] Nambu Yoichiro Institute of Theoretical and Experimental Physics (NITEP), Osaka City University, Sumiyoshi-ku, Osaka City, Osaka 558-8585, Japan
[205] Institute of Space and Astronautical Science (JAXA), Chuo-ku, Sagamihara City, Kanagawa 252-0222, Japan
[206] Directorate of Construction, Services & Estate Management, Mumbai 400094, India
[207] Vanderbilt University, Nashville, TN 37235, USA
[208] Universiteit Antwerpen, Prinsstraat 13, B-2000 Antwerpen, Belgium
[209] University of Białystok, 15-424 Białystok, Poland
[210] Department of Physics, Ewha Womans University, Seodaemun-gu, Seoul 03760, Republic of Korea
[211] National Astronomical Observatories, Chinese Academic of Sciences, Chaoyang District, Beijing, People's Republic of China
[212] School of Astronomy and Space Science, University of Chinese Academy of Sciences, Chaoyang District, Beijing, People's Republic of China
[213] University of Southampton, Southampton SO17 1BJ, UK
[214] Institute for Cosmic Ray Research (ICRR), The University of Tokyo, Kashiwa City, Chiba 277-8582, Japan
[215] Chung-Ang University, Seoul 06974, Republic of Korea
[216] Institut de Física d'Altes Energies (IFAE), Barcelona Institute of Science and Technology, and ICREA, E-08193 Barcelona, Spain
[217] Graduate School of Science, Tokyo Institute of Technology, Meguro-ku, Tokyo 152-8551, Japan
[218] University of Washington Bothell, Bothell, WA 98011, USA
[219] Institute of Applied Physics, Nizhny Novgorod, 603950, Russia
[220] Ewha Womans University, Seoul 03760, Republic of Korea
[221] Inje University Gimhae, South Gyeongsang 50834, Republic of Korea
[222] Department of Physics, Myongji University, Yongin 17058, Republic of Korea
[223] Korea Astronomy and Space Science Institute, Daejeon 34055, Republic of Korea
[224] National Institute for Mathematical Sciences, Daejeon 34047, Republic of Korea
[225] Ulsan National Institute of Science and Technology, Ulsan 44919, Republic of Korea
[226] Department of Physical Science, Hiroshima University, Higashihiroshima City, Hiroshima 903-0213, Japan
[227] School of Physics and Astronomy, Cardiff University, Cardiff, CF24 3AA, UK
[228] Institute of Astronomy, National Tsing Hua University, Hsinchu 30013, Taiwan
[229] Bard College, 30 Campus Rd, Annandale-On-Hudson, NY 12504, USA
[230] Institute of Mathematics, Polish Academy of Sciences, 00656 Warsaw, Poland
[231] National Center for Nuclear Research, 05-400 Świerk-Otwock, Poland
[232] Instituto de Fisica Teorica, 28049 Madrid, Spain
[233] Department of Physics, Nagoya University, Chikusa-ku, Nagoya, Aichi 464-8602, Japan
[234] Université de Montréal/Polytechnique, Montreal, Quebec H3T 1J4, Canada
[235] Laboratoire Lagrange, Université Côte d'Azur, Observatoire Côte d'Azur, CNRS, F-06304 Nice, France
[236] Department of Physics, Hanyang University, Seoul 04763, Republic of Korea
[237] Sungkyunkwan University, Seoul 03063, Republic of Korea
[238] NAVIER, École des Ponts, Univ Gustave Eiffel, CNRS, Marne-la-Vallée, France
[239] Department of Physics, National Cheng Kung University, Tainan City 701, Taiwan
[240] National Center for High-performance computing, National Applied Research Laboratories, Hsinchu Science Park, Hsinchu City 30076, Taiwan
[241] Institute for High-Energy Physics, University of Amsterdam, Science Park 904, 1098 XH Amsterdam, Netherlands
[242] NASA Marshall Space Flight Center, Huntsville, AL 35811, USA
[243] University of Washington, Seattle, WA 98195, USA
[244] Dipartimento di Matematica e Fisica, Università degli Studi Roma Tre, I-00146 Roma, Italy
[245] INFN, Sezione di Roma Tre, I-00146 Roma, Italy
[246] ESPCI, CNRS, F-75005 Paris, France
[247] Concordia University Wisconsin, Mequon, WI 53097, USA
[248] Università di Camerino, Dipartimento di Fisica, I-62032 Camerino, Italy

[249] School of Physics Science and Engineering, Tongji University, Shanghai 200092, People's Republic of China
[250] Southern University and A&M College, Baton Rouge, LA 70813, USA
[251] Centre Scientifique de Monaco, 8 quai Antoine Ier, MC-98000, Monaco
[252] Institute for Photon Science and Technology, The University of Tokyo, Bunkyo-ku, Tokyo 113-8656, Japan
[253] Indian Institute of Technology Madras, Chennai 600036, India
[254] Saha Institute of Nuclear Physics, Bidhannagar, West Bengal 700064, India
[255] The Applied Electromagnetic Research Institute, National Institute of Information and Communications Technology (NICT), Koganei City, Tokyo 184-8795, Japan
[256] Institut des Hautes Etudes Scientifiques, F-91440 Bures-sur-Yvette, France
[257] Faculty of Law, Ryukoku University, Fushimi-ku, Kyoto City, Kyoto 612-8577, Japan
[258] Indian Institute of Science Education and Research, Kolkata, Mohanpur, West Bengal 741252, India
[259] Department of Astrophysics/IMAPP, Radboud University Nijmegen, P.O. Box 9010, 6500 GL Nijmegen, Netherlands
[260] Department of Physics, University of Notre Dame, Notre Dame, IN 46556, USA
[261] Consiglio Nazionale delle Ricerche—Istituto dei Sistemi Complessi, Piazzale Aldo Moro 5, I-00185 Roma, Italy
[262] Korea Astronomy and Space Science Institute (KASI), Yuseong-gu, Daejeon 34055, Republic of Korea
[263] Hobart and William Smith Colleges, Geneva, NY 14456, USA
[264] International Institute of Physics, Universidade Federal do Rio Grande do Norte, Natal RN 59078-970, Brazil
[265] Museo Storico della Fisica e Centro Studi e Ricerche "Enrico Fermi", I-00184 Roma, Italy
[266] Lancaster University, Lancaster LA1 4YW, UK
[267] Università di Trento, Dipartimento di Matematica, I-38123 Povo, Trento, Italy
[268] Indian Institute of Science Education and Research, Pune, Maharashtra 411008, India
[269] Dipartimento di Fisica, Università degli Studi di Torino, I-10125 Torino, Italy
[270] Indian Institute of Technology, Palaj, Gandhinagar, Gujarat 382355, India
[271] Department of Physics, Kyoto University, Sakyou-ku, Kyoto City, Kyoto 606-8502, Japan
[272] Department of Electronic Control Engineering, National Institute of Technology, Nagaoka College, Nagaoka City, Niigata 940-8532, Japan
[273] Departamento de Matemática da Universidade de Aveiro and Centre for Research and Development in Mathematics and Applications, Campus de Santiago, 3810-183 Aveiro, Portugal
[274] Marquette University, 11420 W. Clybourn St., Milwaukee, WI 53233, USA
[275] Graduate School of Science and Engineering, Hosei University, Koganei City, Tokyo 184-8584, Japan
[276] Faculty of Science, Toho University, Funabashi City, Chiba 274-8510, Japan
[277] Faculty of Information Science and Technology, Osaka Institute of Technology, Hirakata City, Osaka 573-0196, Japan
[278] Università di Firenze, Sesto Fiorentino I-50019, Italy
[279] INAF, Osservatorio Astrofisico di Arcetri, Largo E. Fermi 5, I-50125 Firenze, Italy
[280] Indian Institute of Technology Hyderabad, Sangareddy, Khandi, Telangana 502285, India
[281] iTHEMS (Interdisciplinary Theoretical and Mathematical Sciences Program), The Institute of Physical and Chemical Research (RIKEN), Wako, Saitama 351-0198, Japan
[282] INAF, Osservatorio di Astrofisica e Scienza dello Spazio, I-40129 Bologna, Italy
[283] Department of Space and Astronautical Science, The Graduate University for Advanced Studies (SOKENDAI), Sagamihara City, Kanagawa 252-5210, Japan
[284] Andrews University, Berrien Springs, MI 49104, USA
[285] Research Center for Space Science, Advanced Research Laboratories, Tokyo City University, Setagaya, Tokyo 158-0082, Japan
[286] Institute for Cosmic Ray Research (ICRR), Research Center for Cosmic Neutrinos (RCCN), The University of Tokyo, Kashiwa City, Chiba 277-8582, Japan
[287] National Metrology Institute of Japan, National Institute of Advanced Industrial Science and Technology, Tsukuba City, Ibaraki 305-8568, Japan
[288] Dipartimento di Scienze Aziendali—Management and Innovation Systems (DISA-MIS), Università di Salerno, I-84084 Fisciano, Salerno, Italy
[289] Van Swinderen Institute for Particle Physics and Gravity, University of Groningen, Nijenborgh 4, 9747 AG Groningen, Netherlands
[290] Faculty of Science, Department of Physics, The Chinese University of Hong Kong, Shatin, N.T., Hong Kong
[291] Vrije Universiteit Brussel, Boulevard de la Plaine 2, B-1050 Ixelles, Belgium
[292] Department of Communications Engineering, National Defense Academy of Japan, Yokosuka City, Kanagawa 239-8686, Japan
[293] Department of Physics, University of Florida, Gainesville, FL 32611, USA
[294] Department of Information and Management Systems Engineering, Nagaoka University of Technology, Nagaoka City, Niigata 940-2188, Japan
[295] Vrije Universiteit Amsterdam, 1081 HV Amsterdam, Netherlands
[296] Department of Physics and Astronomy, Sejong University, Gwangjin-gu, Seoul 143-747, Republic of Korea
[297] Department of Electrophysics, National Chiao Tung University, Hsinchu, Taiwan
[298] Department of Physics, Rikkyo University, Toshima-ku, Tokyo 171-8501, Japan
[299] Jodrell Bank Centre for Astrophysics, School of Physics and Astronomy, University of Manchester, Manchester, M13 9PL, UK
[300] Astrophysics Science Division, NASA's Goddard Space Flight Center, Greenbelt, MD 20771, USA
[301] Columbia Astrophysics Laboratory, Columbia University, 550 West 120th Street, New York, NY 10027, USA
[302] Laboratoire de Physique et Chimie de l'Environnement et de l'Espace, Université d'Orléans/CNRS, F-45071 Orléans Cedex 02, France
[303] Station de radioastronomie de Nançay, Observatoire de Paris, CNRS/INSU, F-18330 Nançay, France
[304] Department of Physics and Astronomy, University of British Columbia, 6224 Agricultural Road, Vancouver, BC V6T 1Z1, Canada
[305] RIKEN Cluster for Pioneering Research, 2-1 Hirosawa, Wako, Saitama 351-0198, Japan
[306] Departamento de Física, Universidad de Santiago de Chile, 9170124 Estación Central, Chile
[307] Center for Interdisciplinary Research in Astrophysics and Space Sciences, Universidad de Santiago de Chile, Santiago, Chile
[308] Department of Physics and Astronomy, West Virginia University, P.O. Box 6315, Morgantown, WV 26506, USA
[309] Center for Gravitational Waves and Cosmology, West Virginia University, Chestnut Ridge Research Building, Morgantown, WV 26505, USA
[310] Center for Computational Astrophysics, Flatiron Institute, 162 5th Avenue, New York, NY 10010, USA
[311] Department of Physics, University of Connecticut, 196 Auditorium Road, U-3046, Storrs, CT 06269-3046, USA
[312] IRAP, CNRS, 9 avenue du Colonel Roche, BP 44346, F-31028 Toulouse Cedex 4, France
[313] Université de Toulouse, CNES, UPS-OMP, F-31028 Toulouse, France
[314] Los Alamos National Laboratory, Los Alamos, NM 87545, USA
[315] SRON-Netherlands Institute for Space Research, Niels Bohrweg 4, 2333 CA, Leiden, Netherlands
[316] Centre for Astrophysics and Supercomputing, Swinburne University of Technology, Hawthorn, VIC, 3122, Australia
[317] CSIRO, Space and Astronomy, P.O. Box 76, Epping, NSW, 1710, Australia
[318] Canadian Institute for Theoretical Astrophysics, University of Toronto, 60 St. George Street, Toronto, ON M5S 3H8, Canada
[319] Dunlap Institute for Astronomy & Astrophysics, University of Toronto, 50 St. George Street, Toronto, ON M5S 3H4, Canada
[320] School of Natural Sciences, University of Tasmania, Hobart, Australia
[321] ARC Centre of Excellence for Gravitational Wave Discovery (OzGrav), Australia

[322] Department of Physics, McGill University, 3600 rue University, Montréal, QC H3A 2T8, Canada
[323] McGill Space Institute, McGill University, 3550 rue University, Montréal, QC H3A 2A7, Canada
[324] LUTH, Observatoire de Paris, PSL Research University, CNRS, Université Paris Diderot, Sorbonne Paris Cité, F-92195 Meudon, France
Received 2021 December 20; revised 2022 March 20; accepted 2022 March 21; published 2022 June 27

Abstract

Isolated neutron stars that are asymmetric with respect to their spin axis are possible sources of detectable continuous gravitational waves. This paper presents a fully coherent search for such signals from eighteen pulsars in data from LIGO and Virgo's third observing run (O3). For known pulsars, efficient and sensitive matched-filter searches can be carried out if one assumes the gravitational radiation is phase-locked to the electromagnetic emission. In the search presented here, we relax this assumption and allow both the frequency and the time derivative of the frequency of the gravitational waves to vary in a small range around those inferred from electromagnetic observations. We find no evidence for continuous gravitational waves, and set upper limits on the strain amplitude for each target. These limits are more constraining for seven of the targets than the spin-down limit defined by ascribing all rotational energy loss to gravitational radiation. In an additional search, we look in O3 data for long-duration (hours–months) transient gravitational waves in the aftermath of pulsar glitches for six targets with a total of nine glitches. We report two marginal outliers from this search, but find no clear evidence for such emission either. The resulting duration-dependent strain upper limits do not surpass indirect energy constraints for any of these targets.

Key words: Gravitational wave astronomy – Neutron stars – Pulsars

1. Introduction

Continuous gravitational waves (CWs) are quasi-monochromatic signals expected to be ever-present in the data of gravitational-wave (GW) detectors such as Advanced LIGO (Aasi et al. 2015a) and Advanced Virgo (Acernese et al. 2015). While the observation of transient GWs from compact binary coalescences has become nearly commonplace (Abbott et al. 2021a), CWs have yet to be detected as of the third observing run (O3). One of the most enticing and commonly sought after sources of CWs is a rapidly spinning, asymmetric neutron star (NS); see Sieniawska & Bejger (2019) and Haskell & Schwenzer (2020) for recent reviews. In the case of a triaxial NS, CW emission occurs at twice the rotation frequency of the star.

Many NSs are observed as pulsars by radio, X-ray, or γ-ray telescopes (Lorimer & Kramer 2012). Pulsars can often be timed extremely precisely—in the best cases, the arrival of new pulses can be predicted to within tens of nanoseconds. This precision can enable exciting science, including sensitive tests of general relativity (Wex & Kramer 2020), placing constraints on the equation of state of the dense matter inside NSs (Lattimer & Prakash 2004; Kramer & Wex 2009; Ho et al. 2015), and using deviations in timing residuals of pulsars to search for a stochastic gravitational-wave background (Verbiest et al. 2016; Arzoumanian et al. 2020; Goncharov et al. 2021). Detecting GWs from spinning NSs would add a completely new messenger to the study of these extreme objects (Glampedakis & Gualtieri 2018; Haskell & Schwenzer 2020).

In this paper, we search in LIGO–Virgo O3 data (taken in 2019–2020) for CWs from NSs that have been observed as pulsars and precisely timed in either the radio or X-ray bands. We identify 18 promising candidates for which the observed spin-down (negative frequency derivative) implies indirect limits on CW emission that fall within a factor of 3 of the expected sensitivity of the search. Some other analyses assume the phase of CWs to be locked to the rotational phase of the crust of the star as observed by electromagnetic (EM) telescopes (Aasi et al. 2014; Abbott et al. 2017a, 2018, 2019a, 2020b, 2021b, 2021e; Nieder et al. 2020; Ashok et al. 2021). Here, we relax that assumption and allow for the frequency of rotation—and its derivative—to differ from the EM-observed values by a small factor: the so-called "narrow-band" search approach (Abbott et al. 2008, 2017b, 2019b; Aasi et al. 2015b; Nieder et al. 2020; Ashok et al. 2021). We use two separate analysis pipelines, the $5n$-vector (Astone et al. 2014; Mastrogiovanni et al. 2017) and the frequency-domain $\mathcal{F}$-statistic (Jaranowski et al. 1998; Wette et al. 2018a) pipelines, to perform phase-coherent searches for CWs on O3 data over our widened parameter space. Using two separate pipelines allows us to cross-check results between pipelines, compare limits set by the two methods, and increase confidence in any potential detection by requiring both pipelines to see the same signal.

A scenario where GW and EM emission have similar, but slightly different phase evolution is plausible, e.g., when there is differential rotation between the rigid crust and superfluid parts of the star. Possible observational evidence for this comes, for example, from pulsar glitches (Link et al. 1992, 2000; Lyne et al. 2000; Fuentes et al. 2017; Haskell 2017): sudden spin-up events that are often followed by an exponential relaxation back to the simple spin-down scenario. In many models (Haskell & Melatos 2015), the superfluid and non-superfluid components build up a lag with respect to one another, and a glitch represents the sudden recoupling of the two components (Anderson & Itoh 1975; Lyne et al. 2000).

Glitches are also directly relevant for GW searches: first, some of our CW search targets glitched during O3. For these, we perform separate phase-coherent searches covering the parts of O3 before and after the glitches. Second, it is also possible that glitches trigger increased GW emission in their aftermath (van Eysden & Melatos 2008; Bennett et al. 2010;

[325] Deceased, 2020 August.

Prix et al. 2011; Melatos et al. 2015; Singh 2017; Yim & Jones 2020). Hence, we also perform additional searches for long-duration transient CW-like signals with durations from a few hours to four months after observed glitches during (or shortly before) O3, covering nine glitches from six pulsars.

The rest of this paper is structured as follows. We discuss our selection of target pulsars and the EM observations that we use to guide our search in Section 2, and the O3 GW data set in Section 3. In Section 4, we describe our methods of analysis. We present the results of the two CW searches in Section 5. We then cover the detailed setup and the results of the search for GW emission in the aftermath of pulsar glitches in Section 6. In Section 7, we conclude the paper with a discussion of the results obtained by all three analyses, as well as their astrophysical implications. Throughout the rest of the paper, we will often refer to the analyses using the $\mathcal{F}$-statistic and 5n-vector pipelines search over all data as the two "CW" searches, and the search for long-duration transients after glitches as the "transient search."

2. Electromagnetic Data and Target Selection

We start with timing solutions from EM observations of pulsars (also referred to as *ephemerides*), and search in a narrow band in frequency and spin-down, as further described below in Section 4. The widths of the frequency and spin-down search bands are usually larger than the uncertainty in the timing solutions. The observations we use were made in radio and X-ray bands, and were provided by the following observatories: the Canadian Hydrogen Intensity Mapping Experiment (CHIME) (Bandura et al. 2014; Amiri et al. 2021), University of Tasmania's Mount Pleasant Observatory 26 m telescope, the 42 ft telescope and Lovell telescope at Jodrell Bank, the MeerKAT telescope (observations made as part of the MeerTime project; see Bailes et al. 2020), the Nançay Decimetric Radio Telescope, the Neutron Star Interior Composition Explorer (NICER) (Gendreau et al. 2016), and the UTMOST timing program with the Molonglo Observatory Synthesis Telescope (MOST) (Bailes et al. 2017; Jankowski et al. 2018; Lower et al. 2020). The `Tempo` (Nice et al. 2015) and `Tempo2` (Edwards et al. 2006) timing packages were used to fit the model parameters and provide timing solutions.

We select our targets for the CW searches in a manner similar to that of Abbott et al. (2019b), based on the sensitive frequency band of the Advanced LIGO and Virgo detectors and availability of precise ephemerides over the duration of O3 from EM observations. We have analyzed all isolated pulsars, except for one, with a rotation frequency between 10 and 350 Hz and for which the spin-down limit falls within a factor of 3 of the expected sensitivity of the full network over the course of O3. This frequency range includes all the high-value targets identified in Abbott et al. (2021e) for which it could be possible to go below the spin-down limit. Pulsars in this frequency range would produce CWs between 20 and 700 Hz. The only pulsar we do not analyze that satisfies these criteria is PSR J0537–6910, which was analyzed in detail using a narrowband approach to search for r-mode emission in Abbott et al. (2021c) and using a targeted approach in Abbott et al. (2021b). Searches lasting up to 120 days during inter-glitch periods for this pulsar are performed by the post-glitch transient search presented in Sections 4.4 and 6.1.

We estimate the expected sensitivity as

$$h_{\rm sens} = \Theta\sqrt{\frac{S(f)}{T_{\rm obs}}}, \tag{1}$$

where $S(f)$ is the power spectral density as a function of frequency for the LIGO Hanford, LIGO Livingston, and Virgo detectors (H1, L1, and V1, respectively), and $T_{\rm obs}$ is the observing time assuming 11 months of data with respective duty cycles of 75%, 77%, and 76%. The factor $\Theta \sim 30$ encodes the scaling of typical narrowband searches but is a function of the number of templates employed in the analysis (Astone et al. 2014).

On the other hand, the spin-down limit is an indirect upper limit (UL) on the GW amplitude assuming all of a pulsar's rotational energy loss comes in the form of GWs (Jaranowski et al. 1998; Prix 2009). It is given by

$$h_{\rm sd} \approx 2.55 \times 10^{-25}\frac{1\ {\rm kpc}}{d}\sqrt{I_{38}\frac{|\dot{f}_{\rm spin}|}{10^{-13}\ {\rm Hz\ s^{-1}}}\frac{1\ {\rm Hz}}{f_{\rm spin}}}, \tag{2}$$

where I_{38} is the star's moment of inertia in units of 10^{38} kg m^2, $f_{\rm spin}$ is its rotation frequency, and $|\dot{f}_{\rm spin}|$ is the absolute value of its spin-down rate (Abbott et al. 2019b). We have computed spin-down limits according to the most recent distance estimates given in the ATNF catalog (Manchester et al. 2005), version 1.64, and extrapolating the rotational frequencies and spin-down rates to O3. For several pulsars, we have used more recent distance estimates from the literature.

In Table 1, we present a list of targets along with the ranges of GW frequency and spin-down parameters and the corresponding numbers of templates covered for the two pipelines used to conduct the CW searches. We discuss our parameter range choices for each pipeline in Section 4. The observatory yielding the timing solution we use for each source is noted in the far right column.

Two pulsars on our list of CW search targets, PSR J0534+2200 (the Crab) and PSR J1105–6107, glitched during O3 (Shaw et al. 2021), on 23 July 2019 and 9 April 2019, respectively. One other, PSR J1813–1749, shows marginal evidence for a glitch on or close to 3 August 2019 (Ho et al. 2020b).

For this reason, we perform two separate searches, before and after the estimated glitch epoch, which are identified in Table 1 with the suffixes "bg" and "ag" for "before glitch" and "after glitch," respectively.

For PSR J0534+2200, we use O3 data until the last observation before the glitch. The analysis after the glitch uses data from 10 days after the glitch epoch, accounting for the estimated relaxation time, until the end of O3.

For PSR J1105–6107, we only search after the glitch, because the glitch occurs nearly at the start of the run. The after-glitch search uses data from two days after the estimated glitch until the end of O3. For PSR J1813–1749, we perform two separate searches: one fully coherent search across the full O3 duration, assuming the pulsar did not glitch, and a search before the glitch. No search after the glitch is performed, because the glitch occurs near the end of the EM timing model (although a post-glitch transient search is conducted assuming the timing model remains valid within uncertainties; see below). Further details about these glitches will also be discussed in Section 6.

Table 1
Setup Parameters for Fully Coherent CW Search Pipelines

Name	R.A.	Decl.	f (Hz)	Δf (5v) (Hz)	Δf ($\mathcal{F}$) (Hz)	$\dot{f}$ $\times 10^{-13}$ (Hz s^{-1})	$\Delta\dot{f}$ (5v) $\times 10^{-15}$ (Hz s^{-1})	$\Delta\dot{f}$ ($\mathcal{F}$) $\times 10^{-15}$ (Hz s^{-1})	$\ddot{f}$ $\times 10^{-23}$ (Hz s^{-2})	$\Delta\ddot{f}$ $\times 10^{-23}$ (Hz s^{-2})	$n^{5v}_{\rm total}$ $\times 10^{7}$	$n^{\mathcal{F}}_{\rm total}$ $\times 10^{7}$	References
J0534+2200 bg	$05^{h}34^{m}31\overset{s}{.}97$	$+22°00'52\overset{''}{.}07$	59.241	…	0.24	−7370.0	…	2900.0	2360.0	5.2	…	983.7	a
J0534+2200 ag	$05^{h}34^{m}31\overset{s}{.}97$	$+22°00'52\overset{''}{.}07$	59.241	0.24	0.24	−7370.0	2300.0	2900.0	2360.0	5.2	498.0	9362.0	a
J0711–6830	$07^{h}11^{m}54\overset{s}{.}18$	$-68°30'47\overset{''}{.}37$	364.234	0.72	1.5	−0.00989	2.1	0.004	0.0	0.0	4.391	45.85	b
J0835–4510	$08^{h}35^{m}20\overset{s}{.}52$	$-45°10'34\overset{''}{.}28$	22.371	0.089	0.089	−313.0	130.0	120.0	504.0	0.0	32.9	281.6	c
J1101–6101	$11^{h}01^{m}44\overset{s}{.}96$	$-61°01'39\overset{''}{.}6$	31.846	0.13	0.13	−45.3	19.0	18.0	0.0	0.0	7.026	61.52	d
J1105–6107	$11^{h}05^{m}25\overset{s}{.}71$	$-61°07'55\overset{''}{.}63$	31.644	0.13	0.13	−79.7	32.0	32.0	554.0	35.0	11.64	266.0	e
J1809–1917	$18^{h}09^{m}43\overset{s}{.}13$	$-19°17'38\overset{''}{.}2$	24.166	0.097	0.097	−74.4	32.0	30.0	3.7	0.14	8.886	152.3	a
J1813-1749 bg	$18^{h}13^{m}35\overset{s}{.}11$	$-17°49'57\overset{''}{.}57$	44.703	…	0.18	−1290.0	…	510.0	0.0	0.0	…	92.08	d
J1813-1749 full	$18^{h}13^{m}35\overset{s}{.}11$	$-17°49'57\overset{''}{.}57$	44.703	0.18	0.18	−1290.0	520.0	510.0	0.0	0.0	266.4	2270.0	d
J1828–1101	$18^{h}28^{m}18\overset{s}{.}85$	$-11°01'51\overset{''}{.}72$	27.754	0.11	0.11	−57.0	23.0	23.0	4.23	9.4	7.481	1162.0	a
J1833–0827	$18^{h}33^{m}40\overset{s}{.}26$	$-08°27'31\overset{''}{.}53$	23.449	0.094	0.094	−25.2	11.0	10.0	−0.463	0.082	2.873	242.2	e
J1838–0655	$18^{h}38^{m}3\overset{s}{.}13$	$-06°55'33\overset{''}{.}4$	28.363	0.11	0.11	−199.0	83.0	80.0	67.1	7.8	27.13	555.4	d
J1856+0245	$18^{h}56^{m}50\overset{s}{.}91$	$+02°45'53\overset{''}{.}17$	24.714	0.099	…	−189.0	79.0	…	0.0	0.0	22.42	…	a
J1913+1011	$19^{h}13^{m}20\overset{s}{.}34$	$+10°11'22\overset{''}{.}97$	55.694	0.22	0.22	−52.5	23.0	21.0	−0.321	2.6	15.02	1951.0	a
J1925+1720	$19^{h}25^{m}27\overset{s}{.}06$	$+17°20'27\overset{''}{.}42$	26.434	0.11	0.11	−36.6	15.0	15.0	3.93	6.3	4.538	469.2	a
J1928+1746	$19^{h}28^{m}42\overset{s}{.}55$	$+17°46'29\overset{''}{.}67$	29.097	0.12	0.12	−55.7	23.0	22.0	0.0	0.0	7.845	68.41	a
J1935+2025	$19^{h}35^{m}41\overset{s}{.}94$	$+20°25'40\overset{''}{.}1$	24.955	0.092	0.1	−189.0	79.0	76.0	95.0	3.4	20.99	581.3	a
J1952+3252	$19^{h}52^{m}58\overset{s}{.}21$	$+32°52'40\overset{''}{.}51$	50.587	0.2	0.2	−74.9	32.0	30.0	2.92	0.012	18.61	3908.0	f
J2124–3358	$21^{h}24^{m}43\overset{s}{.}84$	$-33°58'45\overset{''}{.}06$	405.588	0.91	1.6	−0.0169	2.1	0.0068	0.0	0.0	5.595	48.06	g
J2229+6114	$22^{h}29^{m}6\overset{s}{.}57$	$+61°14'10\overset{''}{.}9$	38.709	0.15	0.16	−590.0	240.0	260.0	1170.0	0.0	107.3	1021.0	f

Note. This table lists frequency f and spin-down ($\dot{f}$, $\ddot{f}$) parameters corresponding to twice the rotational parameters in the pulsar ephemerides at the start of the O3 run (2019 April 1 15:00 UTC, MJD 58574.000), as discussed in Section 4.1. Right ascension (R.A.) and declination (decl.) are given in J2000 coordinates. In the column headings, $\mathcal{F}$ stands for the $\mathcal{F}$-statistic search discussed in Section 4.3 and 5v stands for the 5n-vector method discussed in Section 4.2. The suffixes "bg" and "ag" refer to "before" and "after" glitch, respectively, while "full" corresponds to the full run in the case of PSR J1813–1749. Observatories are indicated by letters in the rightmost column, as follows: (a) Jodrell Bank 42ft telescope and Lovell telescope; (b) MeerKAT telescope (part of the MeerTime project) (Bailes et al. 2020); (c) University of Tasmania's Mt. Pleasant Observatory 26 m telescope; (d) NICER (Gendreau et al. 2016); (e) MOST (Bailes et al. 2017; Jankowski et al. 2018; Lower et al. 2020); (f) CHIME (part of the CHIME pulsar project, Bandura et al. 2014; Amiri et al. 2021); (g) Nançay Decimetric Radio Telescope. This table is available online in a machine-readable format (LIGO Scientific Collaboration et al. 2022).

For the post-glitch transient search, we have used information from the glitch catalogs maintained at ATNF (Hobbs et al. 2021) and Jodrell Bank (Espinoza et al. 2011; Shaw et al. 2021; Basu et al. 2022). We have selected six pulsars with GW frequencies $f > 15$ Hz and with glitches observed during (or shortly before) O3: PSR J0534+2200, PSR J0537–6910, PSR J0908–4913, PSR J1105–6107, PSR J1813–1749, and PSR J1826–1334. Another pulsar within our frequency band of interest, PSR J2021+3651, was observed to glitch during O3 by Jodrell Bank, but the glitch time uncertainty is too large to make our transient search setup feasible. As mentioned before, for PSR J1813–1749 it is not certain if a glitch actually occurred (Ho et al. 2020b), but we perform an opportunistic search here with its assumed parameters.

The ephemerides for PSR J0534+2200 and PSR J1826–1334 were provided by Jodrell Bank; a detailed discussion of the PSR J0534+2200 glitch is given in Shaw et al. (2021). Ephemerides for PSR J0908–4913 and PSR J1105–6107 are derived from UTMOST radio observations; these are discussed further in Lower et al. (2019, 2020). A potential ambiguity in timing solutions from periodically scheduled surveys like UTMOST, particularly affecting glitch size estimates, was discussed by Dunn et al. (2021), but for these two targets it has been confirmed that the provided values are correct. For PSR J1813–1749 and PSR J0537–6910, we use NICER X-ray observations as reported in Ho et al. (2020a, 2020b) and Abbott et al. (2021b). Details for all targets will be listed in Section 6.1.

3. GW Data

We analyze GW strain data taken at the LIGO Hanford Observatory (H1), LIGO Livingston Observatory (L1), and Virgo (V1), during their O3 observing run. O3 consisted of two separate sections, separated by a month-long commissioning break. O3a ran from 1 April 2019, 15:00 UTC until 1 October 2019, 15:00 UTC. O3b ran from 1 November 2019, 15:00 UTC, to 27 March 2020, 17:00 UTC. See Buikema et al. (2020) and Acernese et al. (2019) for general descriptions of the respective performances of the LIGO and Virgo detectors during O3. The calibration of this data set and its uncertainty budget are described in Sun et al. (2020, 2021) and Acernese et al. (2022a).

Data preparation for all searches starts with removing times of large transient noise with known causes, referred to as "CAT1" vetoes (Davis et al. 2021; Acernese et al. 2022b), from calibrated strain data.

This procedure removed 0.7 days out of 246 days of H1 data, 2.2 days out of 256 days of L1 data, and 0.46 days out of 251 days of V1 data.

The data are then cleaned to remove some known monochromatic or quasi-monochromatic detector artifacts that can be effectively monitored by external sensors, such as signals injected for calibration, or contamination from power mains (Davis et al. 2019; Sun et al. 2020, 2021; Acernese et al. 2022a, 2022b; Viets & Wade 2021). The H1 and L1 data near the 60 Hz mains power frequency are also cleaned using a nonlinear filtering method outlined in Vajente et al. (2020).

The data from L1 and H1 are then "gated" to remove further large transient artifacts, which removes an additional 1.0 day of data from L1 and 0.62 days of data from H1 (Davis et al. 2021; Zweizig & Riles 2021).

There are some differences in how each search pipeline uses this data, as will also be discussed in detail in Section 4. The $5n$-vector search creates Short Fourier Databases (SFDBs) from the time-domain data. SFDBs consist of a collection of short-duration (1024 s long) fast Fourier transforms (FFTs), overlapped by half and Tukey-windowed with a window shape parameter of $\alpha = 0.001$. During the construction of the SFDBs, an extra time-domain cleaning (see, e.g., Astone et al. 2005, in addition to those discussed in the previous paragraph) is applied to identify delta-like time-domain disturbances. The $\mathcal{F}$-statistic and transient pipelines create 1800 s Tukey-windowed short Fourier transforms (SFTs) with a window shape parameter of $\alpha = 0.001$, and then extract a narrow frequency range around the frequency band for each pulsar.

Additional narrow lines with identified instrumental origin are listed in Goetz et al. (2021) and Piccinni et al. (2021); we use these for pipeline-level cleaning or post-processing vetoes, as discussed in later sections.

4. Signal Model and Search Methods

4.1. Signal Model

With all three pipelines, we search for quasi-monochromatic GW signals with fixed intrinsic amplitude at approximately twice the pulsar rotation frequency, $f \approx 2f_{\rm spin}$, allowing for some deviation in the narrowband search approach. The general frequency evolution model for such GWs, following the standard model for a pulsar's $f_{\rm spin}$ as a function of time t' at the pulsar, is

$$f(t') = f_{\rm Taylor}(t') + f_{\rm glitch}(t'). \tag{3}$$

For most pulsars, no glitches have been observed during O3, and hence only the first term for the long-time spin-down evolution is relevant:

$$f_{\rm Taylor}(t') = \sum_{k=0}^{N} \frac{f^{(k)}(t' - T_{\rm ref})^k}{k!}, \tag{4}$$

with a reference time $T_{\rm ref}$ and up to N frequency derivatives $f^{(k)}$. We will also use $\dot{f}$, $\ddot{f}$, and $\dddot{f}$ for the first three derivatives in this paper. The three search methods in this paper have different maximum values of N that they can handle, as discussed in Appendix A.

For glitching pulsars, the additional term is

$$f_{\rm glitch}(t') = \Theta(t' - T_{\rm gl})\left[\sum_{k=0}^{M} \frac{\Delta f_{\rm gl}^{(k)}(t' - T_{\rm gl})^k}{k!} + \delta f_{\rm R}\, e^{-(t'-T_{\rm gl})/\tau_{\rm R}}\right] \tag{5}$$

(or multiple such terms for pulsars with multiple glitches), where $\Theta(x)$ is the Heaviside step function, $T_{\rm gl}$ is the glitch time, $\Delta f_{\rm gl}^{(k)}$ with $M \leqslant N$ are the permanent jumps in the frequency and its derivatives, $\delta f_{\rm R}$ is the part of the frequency jump that relaxes back, and $\tau_{\rm R}$ is the relaxation time. Relaxation is not necessarily observed for all glitches. The glitch term is typically a small correction on top of $f_{\rm Taylor}(t')$.

Building on this frequency evolution model, the full GW signal received by a detector is

$$h(t) = F_+(t;\, \alpha,\, \delta,\, \psi)h_+(t) + F_\times(t;\, \alpha,\, \delta,\, \psi)h_\times(t), \tag{6}$$

where $F_{+,\times}(t; \alpha, \delta, \psi)$ is the detector response to $+$ and $\times$ polarized GWs received at the detector at time t, coming from R.A. α and decl. δ with polarization angle ψ (Jaranowski et al. 1998). Timing corrections for translating from t' to t are discussed below.

The amplitude of each GW polarization can be written as

$$h_+(t) = \frac{1}{2}h_0(1 + \cos^2\iota)\cos[\phi_0 + \Phi(t; \{f^{(k)}\}, \alpha, \delta)], \quad (7a)$$

$$h_\times(t) = h_0 \cos\iota \sin[\phi_0 + \Phi(t; \{f^{(k)}\}, \alpha, \delta)], \quad (7b)$$

where ι is the inclination angle of the pulsar, ϕ_0 is the initial phase, h_0 is an overall dimensionless strain amplitude as discussed below, and $\Phi(t; \{f^{(k)}\}, \alpha, \delta)$ is the integrated phase from the timing model of Equation (3).

To convert from t' at the source to t at the detector, several timing corrections typically need to be addressed: proper motion of the source, binary orbital motion, and the motion of the detectors around the solar system barycenter. Proper motions between the pulsar and the solar system can usually be ignored (Covas 2020) for these searches, and in this analysis we do not cover sources in binary orbits as in, e.g., Abbott et al. (2021d, 2021e, 2022), Ashok et al. (2021). However, the sky position dependent correction between solar system barycenter and detector frame is a crucial part of the analysis methods described in the following, and is implemented in all cases (Jaranowski et al. 1998).

For GWs from a non-axisymmetric star, the amplitude h_0 can be written as

$$h_0 = \frac{4\pi^2 G}{c^4}\frac{I_{zz} f^2 \epsilon}{d}, \quad (8)$$

where d is the distance to the NS, f is the GW frequency, and I_{zz} is the principal moment of inertia. The ellipticity, ϵ, is given by

$$\epsilon = \frac{|I_{xx} - I_{yy}|}{I_{zz}}. \quad (9)$$

In summary, our CW signal model depends on two sets of parameters: the frequency-evolution parameters $\lambda = \{f^{(k)}, \alpha, \delta\}$, and the amplitude parameters $\mathcal{A} = \{h_0, \cos\iota, \psi, \phi_0\}$. The signal model for the long-duration transient search is also based on the one discussed here, but with an additional window function in time, as will be discussed below in Section 4.4.

For both CW pipelines, we search over a narrow range of GW frequencies and first spin-down terms centered on their respective central estimates from the source ephemeris: $f = 2f_{\rm spin}(1 \pm \kappa)$ and $\dot{f} = 2\dot{f}_{\rm spin}(1 \pm \kappa)$, where we take $\kappa = 2 \times 10^{-3}$. This value is intended to allow for physical offsets between the frequency of EM-observed pulsar rotation and the GW emission process, as discussed in the introduction and in more detail in Abbott et al. (2008, 2019b).

The frequency and spin-down changes due to glitches offer evidence of how large of a physical offset we might expect. While glitches with $\Delta f^{(1)}_{\rm gl}/\dot{f}_{\rm spin} \gtrsim 2 \times 10^{-3}$ are observed occasionally, this value of κ encompasses most glitches that have been observed (see, e.g., Fuentes et al. 2017; Lower et al. 2021), and increasing this value significantly to encompass all observed glitch sizes would not be computationally feasible. The full widths we allow for both parameters, $\Delta f = 4\kappa f_{\rm spin}$ and $\Delta\dot{f} = 4\kappa\dot{f}_{\rm spin}$, are shown in Table 1 for each target we consider. Higher-order frequency derivatives are handled differently by each pipeline, which we discuss in the next two subsections and in Appendix A.

4.2. 5n-vector Narrowband Pipeline

The *5n-vector narrowband pipeline* uses the 5*n*-vector method of Astone et al. (2010, 2012) to search for CWs in a narrow frequency and spin-down range around the source ephemerides. This method searches for the characteristic modulations imprinted by the Earth's rotation on a GW signal, splitting it into five harmonics. The search is applied for the n detectors present in the network. For more details on the implementation of the method we use here, see Mastrogiovanni et al. (2017).

The starting point of the analysis is a collection of 1024 s long FFTs built as explained in the previous section. For each target, we extract a frequency band large enough to contain the Doppler modulation of every template that we consider. When higher-order frequency derivatives are used to fit the EM data, the corresponding GW spin-down terms (including $\ddot{f}$) are fixed to twice the values provided in the source ephemerides.

For each target, we then correct for the Doppler modulation in the time domain using a nonuniform downsampling to 1 Hz. Using this time series, we then apply two matched filters (for the two CW polarizations) and construct a detection statistic S coherently combining the matched filter results from all detectors (Mastrogiovanni et al. 2017) for each template in the f and $\dot{f}$ space. The detection statistic is defined as

$$S = |H_+|^2|A_+|^4 + |H_\times|^2|A_\times|^4, \quad (10)$$

where $A_{+/\times}$ are the Fourier components of $F_{+/\times}(t; \hat{n}, \psi = 0)$ and $H_{+/\times}$ are GW amplitude estimators built from the Fourier components of the data and $A_{+/\times}$. The template bank bin size in frequency is given by the inverse of the time-series duration and the spin-down bin size is given by its inverse squared.

The final step is to select the local maximum of the detection statistic in every 10^{-4} Hz band over all spin-down values considered. Within this set of points in the parameter space, we select as outliers those with a p-value (defined as the tail probability of the detection statistic noise-only distribution) below a 1% threshold, taking into account the number of templates applied in the f–$\dot{f}$ space. The noise-only distribution of the detection statistic used to estimate the threshold for candidate selection is built using all the templates excluded from the analysis in each 10^{-4} Hz band. The detection statistic value corresponding to the threshold for candidate selection is extrapolated from the noise-only distribution using an exponential fit of the tail.

Finally, to compute the 95% confidence level ULs $h_0^{95\%}$ on the CW amplitude in the case of no detection, we perform software injections with simulated GW signals in each 10^{-4} Hz sub-band to estimate the value of h_0 at which we achieve 95% detection efficiency at a false-alarm probability of 1%.

4.3. Frequency-domain $\mathcal{F}$-statistic Pipeline

We also use the frequency-domain $\mathcal{F}$-statistic pipeline to search for CWs in a narrow frequency and spin-down range around the source ephemerides. The $\mathcal{F}$-statistic is a matched filter that is maximized over the amplitude parameters $\mathcal{A}$ of the quasi-monochromatic signals (Jaranowski et al. 1998; Cutler & Schutz 2005); see Tenorio et al. (2021a) for a review covering its applications.

For each target, we search over the range of GW frequency f and spin-down $\dot{f}$, with matched-filter templates chosen using the multidetector $\mathcal{F}$-statistic metric (Prix 2007; Wette et al. 2008), which we call through the `LALSuite` (LIGO Scientific Collaboration 2021) program `lalapps_Weave` (Wette et al. 2018a). If the second spin derivative $\ddot{f}_{\rm spin}$ is nonzero, we also search over the range $\ddot{f} = 2(\ddot{f}_{\rm spin} \pm 3\sigma_{\ddot{f}_{\rm spin}})$, where $\sigma_{\ddot{f}_{\rm spin}}$ is the $1\,\sigma$ uncertainty given in the source ephemeris. Higher-order frequency derivatives, up to $f^{(4)}$, are fixed to the EM-measured values. Because of constraints on the pipeline infrastructure, if the source ephemeris for a target includes derivatives above $f^{(4)}$, we refit the arrival times with fewer frequency derivatives. This results in slightly different ephemerides being used for this search and for the 5n-vector search. We discuss targets for which this is the case in Appendix A.

We place templates with a maximum matched-filter mismatch from a putative source of 0.02, which leads to a very dense grid compared to the one used by the 5n-vector search. This can be seen by comparing the final two (non-reference) columns of Table 1. The analysis uses a set of 1800 s Tukey-windowed SFTs over the full data span for all three detectors, and produces a detection statistic, which we denote $2\mathcal{F}$, for each matched-filter template. See Section 3 for a full discussion of data processing and data quality cuts made before generation of the SFTs.

Following Tenorio et al. (2022), we construct 10^4 randomly chosen batches of templates from our search results for each pulsar, and fit a Gumbel distribution to the distribution of the maxima of these batches. We can then propagate this Gumbel distribution based on the total number of templates to estimate the tail probability (p-value) of the largest template across the full search for that target. We outline our implementation of this method more fully in Appendix B.1.

If any templates have a p-value of less than 1% and corresponding large $2\mathcal{F}$ values, we perform follow-up studies of these templates. A list of frequencies of known narrow spectral artifacts, $f_{\rm l}$, and their nominal widths, $w_{\rm l}$, are collated for all three detectors (Goetz et al. 2021; Piccinni et al. 2021). If $|f_{\rm l} - f_{\rm large}| < w_{\rm l}$, where $f_{\rm large}$ is the frequency of the large-$2\mathcal{F}$ template, then we veto that template. We also look at the single-detector $2\mathcal{F}$ value calculated for each detector. If the individual $2\mathcal{F}$ value for such a template in a single detector is larger than the $2\mathcal{F}$ value calculated using the whole network, then we also veto that large-$2\mathcal{F}$ template (Keitel et al. 2014; Leaci 2015). Any remaining large-$2\mathcal{F}$ templates with $p < 1\%$ are then flagged for further follow-up, and could be considered candidates for detection (subject to further studies).

In the absence of a detection, we set ULs at 95% confidence, $h_0^{95\%}$, for each target using the software-injection scheme set out in, e.g., Abbott et al. (2007).

4.4. Post-glitch Transient Search

The search for long-duration transient CW-like signals from glitching pulsars is motivated by the idea that some of the excess energy liberated in a glitch could correspond to transient changes in the quadrupole moment of the star and be radiated away in GWs (van Eysden & Melatos 2008; Bennett et al. 2010; Prix et al. 2011; Melatos et al. 2015; Singh 2017; Yim & Jones 2020) during the post-glitch relaxation phase.

To search for such signals, we use the transient $\mathcal{F}$-statistic method introduced by Prix et al. (2011) and previously applied to LIGO O2 data in searches for GWs from glitches in the Crab and Vela pulsars (Keitel et al. 2019). The idea is to search for long-duration transients that are "CW-like" in the sense of following the standard quasi-monochromatic CW signal model from Section 4.1 with only an additional window function $\varpi(t; t_0, \tau)$ in time applied:

$$h(t;\, \lambda,\, \mathcal{A},\, \mathcal{T}) = \varpi(t;\, t_0,\, \tau) h(t;\, \lambda,\, \mathcal{A}), \tag{11}$$

where the transient parameters $\mathcal{T}$ consist of the window shape, signal start time t_0, and a duration parameter τ. As in Keitel et al. (2019), we limit ourselves here to the simplest case of rectangular windows, meaning the signal is exactly a standard CW that starts at time t_0 and is cut off at time $t_0 + \tau$, with no additional amplitude evolution. Some form of amplitude decay would be expected for a realistic signal linked to post-glitch relaxation (Yim & Jones 2020). As demonstrated in Prix et al. (2011) and Keitel et al. (2019), the signal-to-noise ratio (S/N) loss from using rectangular windows in a search for exponentially decaying signals is mild, while using exponentially windowed search templates would mean a much higher computational cost (Keitel & Ashton 2018).

The search uses the same underlying $\mathcal{F}$-statistic library functions in `LALSuite` (LIGO Scientific Collaboration 2021) as the CW search described in Section 4.3, analyzing SFT data with the `lalapps_ComputeFstatistic_v2` program that has been used before in, e.g., searches for CWs from supernova remnants (Aasi et al. 2015c; Abbott et al. 2019c; Lindblom & Owen 2020). For each target, we perform a search at a fixed sky location over a grid in $f^{(k)}$ parameters, with the number of spin-down terms depending on the pulsar ephemerides, going up to at most a $\ddot{f}$ term. At each grid point λ, the standard multidetector $\mathcal{F}$-statistic is calculated over the maximum duration of interest. Intermediate per-SFT quantities from this calculation, the so-called $\mathcal{F}$-statistic atoms, are kept. As described in Prix et al. (2011), partial sums of these atoms are evaluated in a loop over a range of $\{t_0, \tau\}$. The resulting matrix of $\mathcal{F}_{mn} = \mathcal{F}(t_{0m}, \tau_n)$ statistics gives the likelihoods of transient CW-like signals in each time range. We marginalize $\mathcal{F}_{mn}$ over uniform priors on t_0 and τ, obtaining the Bayes factor $B_{\rm tS/G}$ for transient CW-like signals against Gaussian noise as our detection statistic. As demonstrated by Prix et al. (2011), $B_{\rm tS/G}$ improves detection efficiency compared to taking the maximum of $\mathcal{F}_{mn}$, and as demonstrated by Tenorio et al. (2022), it also produces cleaner background distributions on real data. The computational cost of these searches scales linearly with the number of λ templates and with the product of the numbers of t_0 and τ values, and is dominated by the partial summing steps over the latter two parameters. See Prix et al. (2011) and Keitel & Ashton (2018) for details.

As this is only the second search thus far for long-transient GWs of this type (after Keitel et al. 2019), we describe its practical setup in more detail in Section 6.1.

5. CW Search Results

As described below, we find no significant candidates, although both the $\mathcal{F}$-statistic and 5n-vector CW searches find outliers requiring further follow up after the vetoes in Section 4 were applied. Hence, we set observational ULs on the GW strain from each target, constraining GW emission below the spin-down limit on 7 of the 18 target pulsars. All UL results are shown in Figure 1, and listed in Table 2. We give details of the

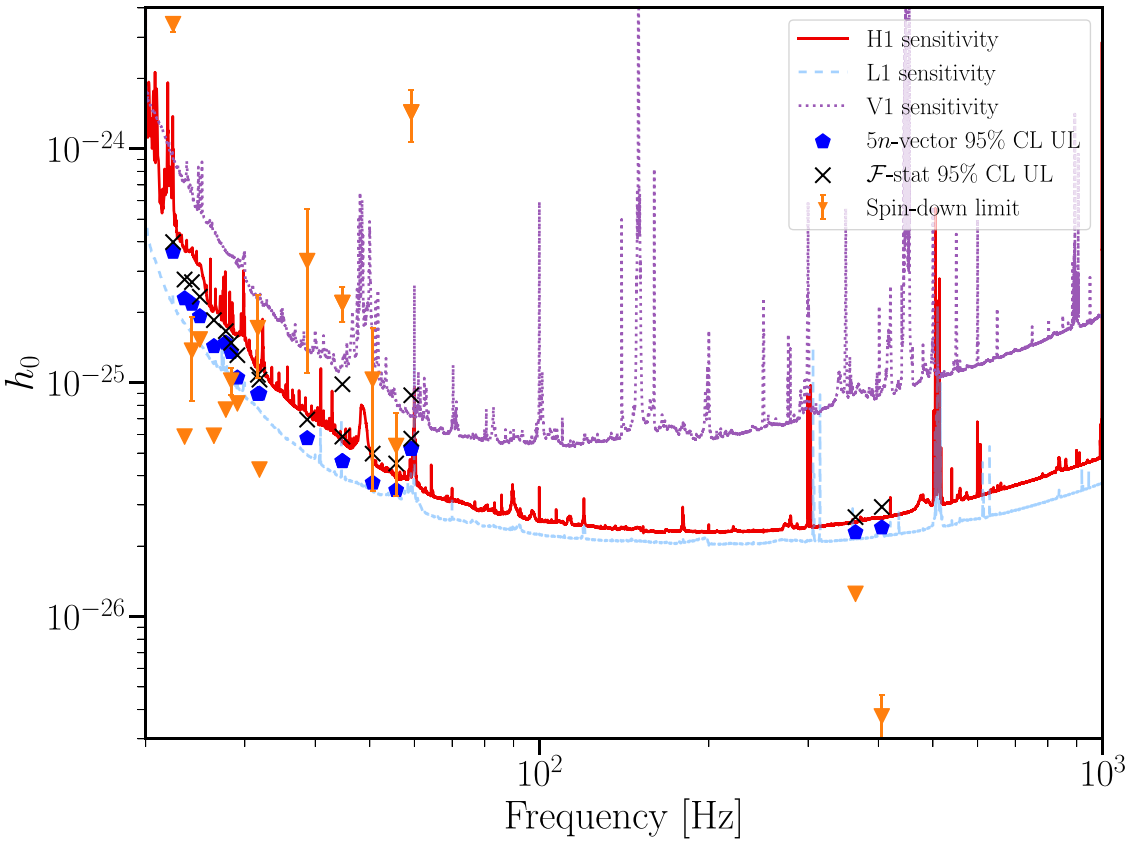

Figure 1. The red solid, blue dashed, and purple dotted curves show the expected sensitivities for H1, L1, and V1, respectively, using Equation (1). The blue pentagons indicate the median 95% CL ULs from the 5*n*-vector search across all 10^{-4} Hz sub-bands for each source. The black crosses indicate 95% CL ULs from the $\mathcal{F}$-statistic search, which are set across the full search range for each target. The orange triangles indicate the spin-down limit, $h_{\rm sd}$, with error bars that reflect uncertainty in the distance to each source. In a few cases, the error bars are smaller than the size of the markers. We discuss and compare these limits in more detail in Section 7. We do not show uncertainties on ULs here, although we discuss uncertainties due to the UL-setting method as well as calibration uncertainties in Section 7. The data for this figure are available online (LIGO Scientific Collaboration et al. 2022).

results from both pipelines, including outliers that were followed up, in the rest of this section.

When discussing ULs in the following section, it should be noted that physically meaningful constraints on the GW energy emission are set when the ULs are lower than the spin-down limit (i.e., when the limit has been *surpassed*). Ellipticity constraints for pulsars whose spin-down limit is not surpassed would imply a $|\dot{f}_{\rm spin}|$ higher than the one observed.

Finally, distance estimates used for the spin-down limits are given in Table 2. These are either from the ATNF pulsar catalog (based on dispersion measures) or from the literature. For the pulsar PSR J1813–1749, different models of the electron density in the Galaxy yield different distance estimates (Camilo et al. 2021). We have used the more optimistic estimate $d = 6.2 \pm 2.4$ kpc, although a different model gives a more pessimistic estimate of $d = 12$ kpc.

5.1. 5n-vector Narrowband Pipeline

The 5*n*-vector pipeline found outliers only for two targets: PSR J1828–1101 and PSR J1838–0655. Figures 2 and 3 show the distribution of outliers in the searched frequency band (marginalized over the spin-down plane), along with the power spectral density (PSD) for each of the three detectors in that band. For PSR J1828–1101, we find 10 outliers around 27.7116 Hz with *p*-values between 10^{-5} and 10^{-2}, and for PSR J1838–0655, we find 13 outliers around 28.3134 Hz with *p*-values between 10^{-3} and 10^{-2}. The nominal *p*-values we report here assume underlying Gaussian noise, an assumption that can break down in the presence of instrumental artifacts.

These outliers are all due to noise disturbances identified in H1 data. For PSR J1828–1101, the PSDs for each of the three detectors around the outliers are shown in the top panel of Figure 2, while the *S*-statistic, defined in Equation (10), is shown in the middle panel. The outliers are produced by a known noise line at 27.71 Hz with width of 0.02 Hz caused by a resonance in one of the suspended optics at H1. For PSR J1838–0655, the outliers are due to an identified broad noise line of unknown origin (Goetz et al. 2021). The top panel of Figure 3 shows the PSD for each of the three detectors around these outliers. As can be seen, various broad noise disturbances are present in H1 data in the frequency band of PSR J1838–0655. Even if the origin of these noise lines is unknown, we can confidently exclude them as astrophysical CW signals because, if they were real, they would have been present also in the L1 data, which are more sensitive. In Section 5.2, we also perform a dedicated follow-up for the candidates due to these noise disturbances showing that they are only visible in H1 data.

The median ULs across the 10^{-4} Hz sub-bands, $h_0^{95\%}$, for each pulsar are shown in column 3 of Table 2 and plotted with blue pentagons in Figure 1. The ratio of the UL with $h_{\rm sd}$ is shown in column 6 of Table 2, and the limits on the ellipticity of the pulsar are shown in column 8. We discuss and compare these limits to those of the $\mathcal{F}$-statistic pipeline, to previous

Table 2
UL Results on CW Strain from the $5n$-vector (5v) and $\mathcal{F}$-statistic ($\mathcal{F}$) Pipelines.

Name	f (Hz)	h_0^{95} (5v) $\times 10^{-26}$	h_0^{95} ($\mathcal{F}$) $\times 10^{-26}$	$h_{\rm sd}$ $\times 10^{-26}$	$h_0^{95}/h_{\rm sd}$ (5v)	$h_0^{95}/h_{\rm sd}$ ($\mathcal{F}$)	ϵ (5v) $\times 10^{-5}$	ϵ ($\mathcal{F}$) $\times 10^{-5}$	$\epsilon_{\rm sd}$ $\times 10^{-5}$	d (kpc)	σ_d (kpc)
J0534+2200 bg	59.24	...	8.79	143.0	...	0.061	...	4.6	76.0	2.00 [a]	0.5
J0534+2200 ag	59.24	5.2	6.09	143.0	0.036	0.043	2.7	3.2	76.0	2.00 [a]	0.5
J0711–6830	364.23	2.29	2.69	1.25	1.8	2.2	0.0017	0.002	0.00095	0.11	0.041
J0835–4510	22.37	36.2	39.5	341.0	0.11	0.12	19.0	21.0	180.0	0.28 [b]	0.02
J1101–6101	31.85	8.96	10.5	4.25	2.1	2.5	59.0	68.0	28.0	7.00	2.7
J1105–6107	31.64	8.94	10.1	17.1	0.52	0.59	20.3	23.0	38.0	2.36	0.92
J1809–1917	24.17	21.7	26.1	13.7	1.6	1.9	110.0	140.0	73.0	3.27	1.3
J1813–1749 full	44.70	4.61	5.85	21.9	0.21	0.27	10.0	13.0	64.0	6.20 [c]	2.4
J1813–1749 bg	44.70	...	9.61	21.9	...	0.44	...	21.0	64.0	6.20 [c]	2.4
J1828–1101	27.75	14.8	16.3	7.67	1.9	2.1	87.0	96.0	45.0	4.77	1.9
J1833–0827	23.45	22.9	29.3	5.88	3.9	5.0	180.0	230.0	46.0	4.50	1.8
J1838–0655	28.36	13.2	15.3	10.2	1.3	1.5	100.0	120.0	79.0	6.60 [d]	0.9
J1856+0245	19.35	20.5	...	11.2	1.8	...	200.0	...	110.0	6.32	2.46
J1913+1011	55.69	3.47	4.37	5.36	0.65	0.81	4.9	6.1	7.5	4.61	1.8
J1925+1720	26.43	14.3	17.6	5.93	2.4	3.0	98.0	120.0	41.0	5.06	2.0
J1928+1746	29.10	10.5	13.5	8.15	1.3	1.7	51.0	66.0	39.0	4.34	1.7
J1935+2025	24.95	19.2	23.7	15.3	1.3	1.5	130.0	170.0	110.0	4.60	1.8
J1952+3252	50.59	3.73	4.93	10.3	0.36	0.48	4.1	5.5	11.0	3.00 [e]	2.0
J2124–3358	405.59	2.4	2.9	0.374	6.4	7.7	0.0057	0.0068	0.00095	0.44 [f]	0.05
J2229+6114	38.71	5.78	7.23	33.1	0.17	0.22	11.0	14.0	63.0	3.00 [g]	2.0

Note. We show the ULs on strain amplitude at 95% confidence for both pipelines, h_0^{95}, the spin-down limit for each target $h_{\rm sd}$ along with the implied limit on ellipticity ϵ for each pipeline, and the limit on ellipticity implied by the spin-down limit $\epsilon_{\rm sd}$. Finally, we also show the ratio of the 95% confidence UL and the spin-down limit. We surpass the spin-down limit for seven targets: PSR J0534+2200, PSRJ0835–4510, PSR J1105–6107, PSR J1813–1749, PSR J1913+1011, PSR J1952+3252, and PSR J2229+6114. We do not show uncertainty on ULs here, although we discuss uncertainty due to the UL-setting method as well as calibration uncertainty in Section 7. Distance estimates d and their uncertainties σ_d are from dispersion measures (with a fiducial uncertainty of 40% from Yao et al. 2017) unless noted with one of the following letters: (a) Kaplan et al. (2008); (b) Dodson et al. (2003); (c) Camilo et al. (2021); (d) Gotthelf & Halpern (2008); (e) Verbiest et al. (2012); (f) Reardon et al. (2021); (g) Halpern et al. (2001). This table and a machine-readable file are available online (LIGO Scientific Collaboration et al. 2022).

searches for the same targets, and to the spin-down limits, in Sections 5.3 and 7.

5.2. Frequency-domain $\mathcal{F}$-statistic Pipeline

The $\mathcal{F}$-statistic pipeline identified outliers with p-value < 0.01 that could not be vetoed with the methods described in Section 4.3 for two targets: PSR J1813–1749 bg and PSR J1838–0655. As described in Section 4.3, a first round of vetoes was made where we rejected outliers that were close to known narrow spectral artifacts. This resulted in vetoing outliers in PSR J1828–1101, which are shown in the bottom panel of Figure 2 for completeness and comparison with the $5n$-vector search. We also vetoed outliers with a $2\mathcal{F}$ value that was larger when running on data from a single detector than when running on the full network. In Figures 3 and 4, we show the PSD in the top panel in the search band for the remaining outliers for PSR J1838–0655 and PSR J1813–1749 bg, respectively, while the search pipeline statistic, the $\mathcal{F}$-statistic discussed in Section 4.3, is shown in the bottom panel(s).

The outliers for PSR J1813–1749 bg are associated with an artifact that contaminates the first two weeks of O3. Although it is nearby, it lies outside the nominal width of the line specified in Goetz et al. (2021), which can be seen in Figure 4, and therefore it is unlikely to be explicitly caused by that line. However, in Appendix C, we perform a follow-up study that shows that the outliers in this band increase in significance when running on data only from the first two weeks of the run. This behavior is inconsistent with a CW signal, and so we veto these outliers.

The remaining outliers from PSR J1838–0655, shown in Figure 3, are in the same frequency range as those for the $5n$-vector pipeline. These outliers are all near a clear disturbance in H1, and the $2\mathcal{F}$ value for all of them is larger when running only on H1 data than when running only on L1 data. However, L1 is significantly more sensitive than H1 in the frequency bands of interest. In Appendix C, we detail a follow-up study on the remaining outliers. We show, based on a realistic set of injections, that for a true signal it is very unlikely to have a larger $2\mathcal{F}$ value when running only on H1 data than when running only on L1 data, due to the difference in the sensitivity for the two detectors.

One pulsar, PSR J1856+0245, was in a frequency band that had significant instrumental disturbances, and so we could not reliably estimate the background distribution and do not report ULs (or search results) for it. We discuss this case in Appendix B.1.

Given that there are no remaining candidates that exceed our follow-up threshold, we set ULs at 95% confidence on the strain amplitude, h_0, of a potential CW signal produced by our targets. The UL, calculated across the full parameter space, $h_0^{95\%}$, for each pulsar is shown in column 4 of Table 2 and plotted with black crosses in Figure 1. The ratio $h_0^{95\%}/h_{\rm sd}$ is shown in column 7 of Table 2, and the limit on the ellipticity of each pulsar is shown in column 9. We discuss these limits in detail, and in the context of indirect limits and the $5n$-vector results, in Section 7.

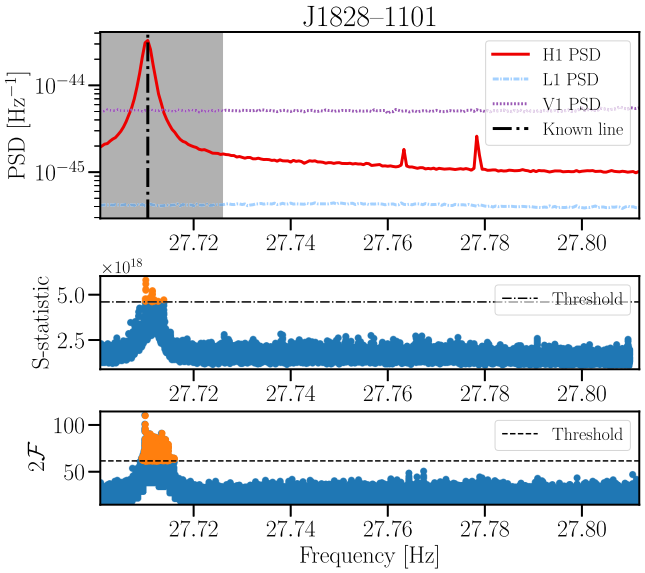

Figure 2. Top panel: Median PSD across the run in each frequency bin for Hanford (red, solid), Livingston (blue, dashed), and Virgo (purple, dotted), for the frequency band searched for PSR J1828–1101. There is an obvious disturbance caused by a resonance in one of the suspended optics at H1, which is marked with the vertical dashed black line. Its estimated width is given by the shaded region. The line is clearly associated with large values of the detection statistics in the two other panels. Middle panel: $\mathcal{S}$-statistic obtained for PSR J1828–1101 in the narrow frequency range explored and marginalized over the spin-down values. The horizontal dashed line indicates the threshold corresponding to a 1% false-alarm rate. The orange markers indicate the outliers found. Bottom panel: $2\mathcal{F}$ obtained for PSR J1828–1101 in the narrow frequency range explored. The horizontal dashed line indicates the threshold corresponding to a 1% false-alarm rate. The orange markers indicate the outliers found and vetoed using the known lines veto.

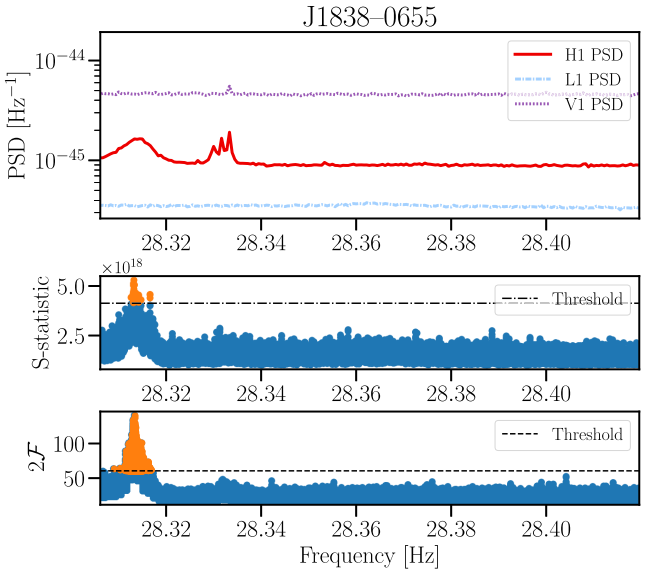

Figure 3. Top panel: Median PSD across the run in each frequency bin for Hanford (red, solid), Livingston (blue, dashed), and Virgo (purple, dotted) for the frequency band searched for PSR J1838–0655. There is an obvious disturbance (of unknown origin) at H1 which is associated with large values of the detection statistics in the two other panels. Middle panel: $\mathcal{S}$-statistic obtained for PSR J1838–1101 in the narrow frequency range explored and marginalized over the spin-down values. The horizontal dashed line indicates the threshold corresponding to a 1% false-alarm rate. The orange markers indicate the outliers found. Bottom panel: $2\mathcal{F}$ obtained for PSR J1838–1101 in the narrow frequency range explored. The horizontal dashed line indicates the threshold corresponding to a 1% false-alarm rate. The orange markers indicate the outliers found. Follow-ups of these outliers are discussed in Appendix C.

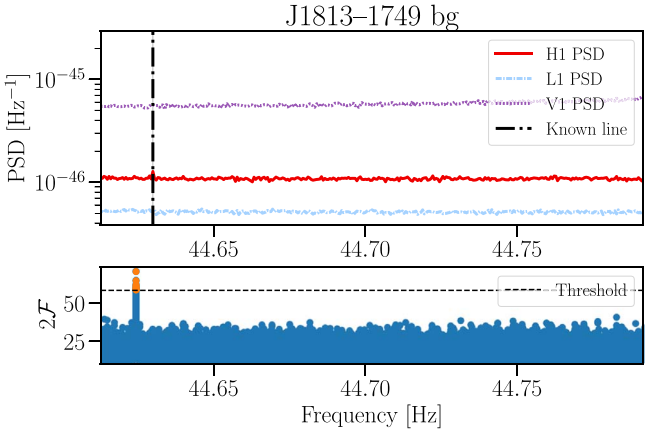

Figure 4. Top panel: Median PSD across the run in each frequency bin for Hanford (red), Livingston (blue), and Virgo (purple) for the frequency band searched for PSR J1813–1749. There is a small bump near a known line in H1 (marked with the vertical dashed line). However, this is distinct from the spike in $2\mathcal{F}$ values shown in the bottom panel. Bottom panel: $2\mathcal{F}$ obtained for PSR J1813–1749 bg in the narrow frequency range explored. The horizontal dashed line indicates the threshold corresponding to a 1% false-alarm rate. The orange markers indicate the outliers found. We were unable to identify this outlier as being due to the known line, but after follow-up detailed in Appendix C, it is clear that these outliers are caused by an artifact that affects the first two weeks of O3.

5.3. Comparison between Pipelines

The ULs from the $\mathcal{F}$-statistic pipeline are, on average, 19% higher than those set by the 5n-vector pipeline. They are not directly comparable, however, as the 5n-vector pipeline results are the median across 10^{-4} Hz sub-bands, while the $\mathcal{F}$-statistic limits are set across the whole parameter space for each pulsar. A more equitable comparison is to compare the largest UL across all sub-bands for the 5n-vector, which is on average 9% lower than the ULs set by the $\mathcal{F}$-statistic pipeline.

A direct comparison would be very involved due to the differing pre-treatment of the data and methods used by the two pipelines. However, there are a few clear methodological differences that could explain the difference in ULs, which we highlight below.

The most obvious difference is in the effective "trials factors" used in generating the thresholds for follow-up, which are then used for the threshold of "detection" when performing the software injections used to calculate ULs. Looking at a larger number of templates reduces the effective mismatch between templates and a signal, but also increases the likelihood of finding a larger detection statistic due to a noise fluctuation. The $\mathcal{F}$-statistic search uses significantly more templates than the 5n-vector pipeline in nearly all cases. Fitting the relationship between the ratio of templates used in the two pipelines to the ratio of their ULs, we find that, for an equal number of templates, the $\mathcal{F}$-statistic search would have limits $\sim 5\%$ higher than the maximum UL compared to the 5n-vector search. This is consistent with the scaling found in Astone et al. (2014). Inevitably, these differences are a reflection of the full range of choices made for the two pipelines, which also include how thresholds for follow-up are set (e.g., the method outlined in Appendix B.1 versus extrapolating the tail of the background distribution), the cleaning procedures used in preparing the data, and the densities of the templates used to perform the searches.

Table 3
Parameters and Transient Search Setups for Five of the Glitching Pulsars

	J0534+2200	J0908–4913	J1105–6107	J1813–1749	J1826–1334
d [pc]	2000 ± 500[a]	1000 ± 390	2360 ± 920.4	6200 ± 2400[b]	3606 ± 1406
R.A.	$05^{h}34^{m}31\overset{s}{.}97$	$09^{h}08^{m}35\overset{s}{.}47$	$11^{h}05^{m}25\overset{s}{.}71$	$18^{h}13^{m}35\overset{s}{.}11$	$18^{h}26^{m}13\overset{s}{.}16$
Decl.	$22°00'52\overset{''}{.}07$	$-49°13'05\overset{''}{.}00$	$-61°07'55\overset{''}{.}63$	$-17°49'57\overset{''}{.}57$	$-13°34'45\overset{''}{.}98$
$T_{\rm gl}$ [s]	1247930924	1254619602	1238824009	1248825618	1264809618
$\Delta T_{\rm gl}$ [days]	0.003	4.488	1.997	1	21
$\Delta f_{\rm gl}/f$	1.24×10^{-8}	2.21×10^{-8}	1.17×10^{-6}	1.34×10^{-7}	2.48×10^{-6}
$\Delta \dot{f}_{\rm gl}/\dot{f}$	1.52×10^{-4}	6.73×10^{-4}	3.53×10^{-3}	...	6.82×10^{-3}
$\Delta \ddot{f}_{\rm gl}/\ddot{f}$	...	...	...	...	...
$T_{\rm ref}$ [s]	1247845509	1256655802	1238651637	1248739243	1262996751
f [Hz]	59.204190	18.722385	31.628009	44.679639	19.691348
Δf [Hz]	0.059234	0.018732	0.031644	0.044702	0.019701
$\dot{f}$ [Hz s^{-1}]	-7.3707×10^{-10}	-2.6526×10^{-12}	-7.9786×10^{-12}	-1.2863×10^{-10}	-1.4650×10^{-11}
$\Delta \dot{f}$ [Hz s^{-1}]	7.3670×10^{-13}	2.6513×10^{-15}	3.5865×10^{-14}	1.3200×10^{-13}	1.1358×10^{-13}
$\ddot{f}$ [Hz s^{-2}]	2.3631×10^{-20}	...	6.2723×10^{-21}	...	8.9844×10^{-22}
$\Delta \ddot{f}$ [Hz s^{-2}]	2.3643×10^{-23}	...	1.1809×10^{-21}	...	7.6842×10^{-24}
$\dddot{f}$ [Hz s^{-3}]	...	...	-5.1143×10^{-28}	...	4.2734×10^{-29}
$\Delta \dddot{f}$ [Hz s^{-3}]	...	...	7.9821×10^{-29}	...	2.3250×10^{-30}
N_λ	3917139	507911	61497	7120630	22753

Notes. This table contains information about the five pulsars with a single post-glitch transient analysis. See Table 4 for the special case of PSR J0537–6910. Distances are taken from the ATNF catalog unless indicated otherwise with a footnote, and all other parameters are derived from the ephemerides as discussed in the text. $\Delta f_{\rm gl}$, $\Delta \dot{f}_{\rm gl}$, and $\Delta \ddot{f}_{\rm gl}$ are the glitch step sizes. For each search, the reference time $T_{\rm ref}$ is chosen to match the earliest SFT data timestamp in $T_{\rm gl} \pm \min(\Delta T_{\rm gl}, 1\ {\rm day})$, and the GW frequency and spin-down parameters f, $\dot{f}$, etc, are extrapolated to this time. Here, Δf, $\Delta \dot{f}$, etc., refer to their corresponding search bandwidths. N_λ is the total number of frequency-evolution parameters covered by each search.
[a] Trimble (1973); Kaplan et al. (2008).
[b] Camilo et al. (2021).

6. Post-glitch Transient Search

6.1. Search Setup

For all six targets in the post-glitch transient searches, we use SFTs of duration 1800 s (as discussed in Section 3) from both LIGO detectors and Virgo, except for PSR J0908–4913 and PSR J1826–1334. The frequency bands searched for these two targets are affected by broadband instrumental disturbances in Virgo. For this analysis, we additionally clean narrow instrumental lines with known instrumental origin (Goetz et al. 2021; Piccinni et al. 2021) before the searches, by replacing affected SFT bins with Gaussian noise matching the PSD in the surrounding range.

Observed parameters and search setups for the five pulsars that have a single known glitch during our time of interest are summarized in Table 3. For the "Big Glitcher" PSR J0537–6910 (Middleditch et al. 2006; Ho et al. 2020a), which was previously considered in searches for persistent CWs in the inter-glitch periods by Fesik & Papa (2020) and Abbott et al. (2021b, 2021c), we perform four separate searches following four observed glitches as illustrated in Figure 5. Corresponding parameters are listed in Table 4.

We derive the ranges of frequency evolution parameters λ and transient parameters $\mathcal{T}$ to be covered in each search from the ephemerides for that pulsar, the uncertainty $\delta T_{\rm gl}$ in the glitch time $T_{\rm gl}$, and the availability of GW data relative to $T_{\rm gl}$. We set a maximum signal duration of $\tau_{\rm max} = 120$ days to be searched for each glitch, guided both by observed glitch recovery times being typically on shorter timescales (Lyne et al. 2000; Espinoza et al. 2011; Yu et al. 2013; Yim & Jones 2020; Lower et al. 2021) and by computational cost constraints (Keitel & Ashton 2018). Signal start times t_0 cover $T_{\rm gl} \pm \max(\delta T_{\rm gl}, 1\ {\rm day})$, and the reference time $T_{\rm ref}$ for the frequency and spin-down parameter grids (again assuming GW emission near twice the rotation period) is set to the earliest SFT timestamp in this range. On each side of the nominal $f^{(k)}$ values extrapolated to $T_{\rm ref}$, the grids cover the maximum of (i) 0.001 times the nominal value (this is one quarter of the width used by the CW searches as described in Section 4.1), (ii) the 1σ fit uncertainties from the ephemerides propagated to $T_{\rm ref}$, and (iii) the glitch step size in that parameter. We place the grids using the metric from Prix (2007) and the template placement algorithm from Wette (2014), as implemented in `lalapps_ComputeFstatistic_v2` and `lalpulsar` (LIGO Scientific Collaboration 2021), with a mismatch parameter of 0.2. The algorithm can add some additional grid points outside the nominal ranges to reduce mismatch near the edges. But for targets with $\ddot{f}$ and higher terms in their timing solution, we strictly limit template placement in all spin-down terms to the nominal range, to limit computational cost. Our resolution in $\mathcal{T}$ is $dt_0 = d\tau = 2\,T_{\rm SFT} = 3600$ s. Due to implementation details of the $\mathcal{F}$-statistic (Prix 2015), the minimum duration is $\tau_{\rm min} = 2\,T_{\rm SFT}$.

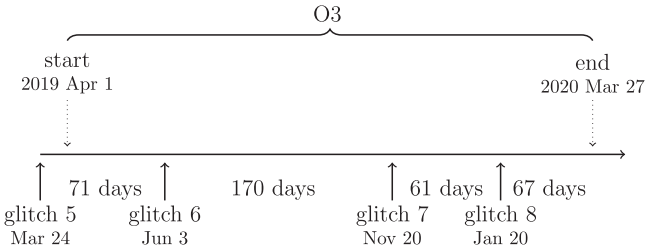

Figure 5. Relative timing of the O3 observing run, the glitches that NICER observed from PSR J0537–6910 (Ho et al. 2020a; Abbott et al. 2021b), and the four post-glitch long-duration transient searches we perform for this target.

Table 4
Parameters of the Four Searches Targeting Glitches of PSR J0537–6910

	Glitch 5	Glitch 6	Glitch 7	Glitch 8
$T_{\rm gl}$ [s]	1237420818	1243555218	1258243218	1263513618
$\Delta T_{\rm gl}$ [days]	5	8	3	5
$\Delta f_{\rm gl}/f$	1.49×10^{-7}	4.36×10^{-7}	1.22×10^{-7}	3.88×10^{-7}
$\Delta \dot{f}_{\rm gl}/\dot{f}$	4.77×10^{-4}	4.34×10^{-4}	1.11×10^{-3}	1.22×10^{-3}
$\Delta \ddot{f}_{\rm gl}/\ddot{f}$	2.00×10^{-1}	-1.34×10^{-1}	4.88	−4.32
$T_{\rm ref}$ [s]	1238166018	1242864932	1257985627	1263081781
f [Hz]	123.767904	123.766064	123.760042	123.758055
Δf [Hz]	0.123830	0.123828	0.123822	0.123820
$\dot{f}$ [Hz s^{-1}]	-3.9990×10^{-10}	-3.9980×10^{-10}	-4.0034×10^{-10}	-4.0017×10^{-10}
$\Delta \dot{f}$ [Hz s^{-1}]	3.9970×10^{-13}	3.9960×10^{-13}	7.3810×10^{-13}	7.3493×10^{-13}
$\ddot{f}$ [Hz s^{-2}]	1.9990×10^{-20}	1.4420×10^{-20}	9.7927×10^{-20}	-9.4572×10^{-20}
$\Delta \ddot{f}$ [Hz s^{-2}]	2.0000×10^{-23}	3.7517×10^{-21}	1.4036×10^{-19}	1.1735×10^{-19}
$\dddot{f}$ [Hz s^{-3}]	...	...	...	...
$\Delta \dddot{f}$ [Hz s^{-3}]	...	...	...	...
N_λ	593911	11474334	15837589	21543992

Note. Here, $d = (49.59 \pm 0.55)$ kpc (Pietrzyński et al. 2019), the R.A. is $05^{\rm h}37^{\rm m}47\overset{\rm s}{.}42$, and the decl. is $69°10'19\overset{''}{.}88$ for all four searches, while the frequency and spin-down parameters are extrapolated to the $T_{\rm ref}$ corresponding to each search. See Table 3 for details on the listed parameters.

In some special cases, we modified the default setup to match the availability of GW data, explaining some apparent anomalies in the configurations listed in Tables 3 and 4. The glitch from PSR J0908–4913 happened in October of 2019, during the maintenance break between O3a and O3b, a month for which no GW data are available. We still search for the standard set of τ up to 120 days after this glitch, but fix t_0 to the first available SFT timestamp after the break—any templates with a different t_0 in the regular band around the glitch time would yield identical detection statistics—and are insensitive to shorter-duration signals in this case. For PSR J1826–1334, O3 ended 84 days after the nominal glitch time, so we shorten the analysis accordingly.

For PSR J0537–6910, as illustrated in Figure 5 and following the numbering from Ho et al. (2020a), we perform searches covering the durations from each of glitches 5–7 until the next glitch, and for glitch 8 we search until the end of O3. Glitch 5 happened in late March of 2019, shortly before the start of O3, and hence, as for PSR J0908–4913, t_0 is fixed to the data start time.

6.2. Results

To determine whether or not there are interesting outliers in the results of each search, for most targets we again follow the procedure described in Tenorio et al. (2022) to empirically estimate the distribution of the expected highest outlier. For two targets, PSR J1105–6107 and PSR J1826–1334, the number of templates is too low for this method to deliver robust results. Instead, for these targets, we use spatial off-sourcing (Isi et al. 2020) to estimate the background distribution and set a threshold. The specific implementations for both cases are explained in Appendix B.2.

For eight of the nine searches, there are no candidates above threshold. The background distribution from the search after the eighth glitch of PSR J0537–6910 is less clean and requires an additional notching step, as discussed in Appendix B.2. We then find two marginal outliers at about 2 and 1 standard deviations, respectively, from the mean of the estimated extreme-value distribution (4% and 14% tail probability). The best-fit signal durations are about 60 and 45 days, respectively. Appendix D lists the full parameters of these outliers and describes additional analyses to follow them up.

In summary, we cannot associate either outlier with any known spectral artifact or single-detector feature in the data. They pass several consistency tests and vetoes, and behave as weak CW-like candidates are expected to in a fully phase-coherent targeted follow-up (Dupuis & Woan 2005; Pitkin et al. 2017) over the corresponding subsets of O3 data. Nevertheless, we do not consider these as promising detection candidates, for two main reasons: first, they would imply a signal with far higher amplitude than allowed by the estimated glitch energy for this target (see discussion of ULs below). Second, their significance is low, compared also with the 1% tail probability thresholds used by the two CW pipelines in this paper. This is reinforced by follow-up $5n$-vector fixed-duration analyses, which recover local S-statistic peaks at the parameters of each outlier, but not as the loudest candidates in the band. Still, we conservatively use a higher threshold (from including the outliers in the background estimate with no notching) in the UL procedure for PSR J0537–6910 glitch 8.

Having identified no convincing detection candidates above threshold for any of the targets, we set ULs on the GW strain after each glitch. As in the search, we assume CW-like signals that are constant over the signal duration τ, and we evaluate the ULs as a function of τ. To do so, we simulate signals following Equation (11) with λ parameters and t_0 drawn uniformly from within the search ranges, several discrete steps in τ and h_0, and the remaining amplitude parameters randomized over their natural ranges. We add these signals to the original SFTs without the spectral cleaning (as described in Section 6.1), redo the cleaning step to ensure any signals falsely dismissed due to cleaning are properly accounted for, and perform small searches over a portion of the original λ grid (0.1 mHz in f and the closest spin-down points) and the full $\mathcal{T}$ range. The $h_0^{95\%}$ ULs are obtained from a sigmoid fit to the recovery fraction $p_{\rm det}$ above the $B_{\rm tS/G}$ threshold from the main search, as a function of injected h_0 at fixed τ. Results for all targets are shown in Figure 6.

We compare these empirical ULs to an indirect constraint derived in Prix et al. (2011) according to the two-fluid model of

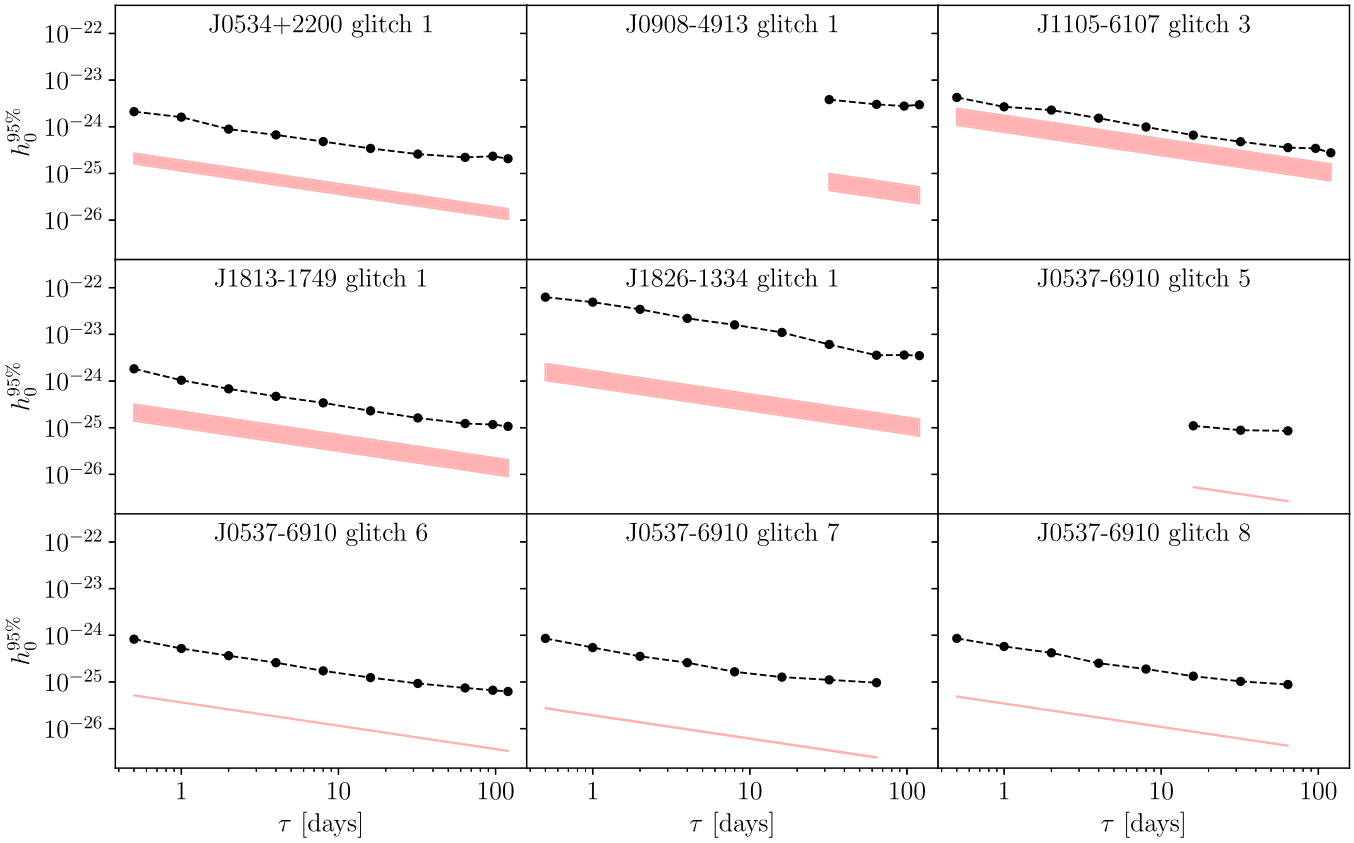

Figure 6. Strain ULs $h_0^{95\%}$ obtained for the six glitching pulsars targeted with the long-duration transient search, as a function of signal duration τ (dashed curves with points representing the injection set). The four searches following glitches in PSR J0537–6910 are shown in separate panels, for readability. Uncertainties from finite injection sample size are at the 3%–5% level, comparable to or lower than amplitude uncertainty from detector calibration as discussed in Section 7. The indirect glitch excess energy ULs from Equation (12), originally derived in Prix et al. (2011) and based on the estimated size of each glitch and distance to the pulsar as listed in Tables 3 and 4, are shown for comparison (red shaded bands). The data for this figure are available online (LIGO Scientific Collaboration et al. 2022).

NS glitches (Lyne et al. 2000). In this model, the excess superfluid energy liberated in a glitch gives a UL to the total GW energy, which corresponds to a τ-dependent strain UL:

$$h_0 \leqslant \frac{1}{d}\sqrt{\frac{5G}{2c^3}\frac{\mathcal{I}}{\tau}\frac{\Delta f_{\rm gl}}{f}}. \tag{12}$$

Qualitatively similar ULs also hold for other glitch models such as crust-cracking starquakes (Middleditch et al. 2006); see again Prix et al. (2011) for details. For the purpose of showing this indirect UL in Figure 6, we have assumed a fiducial moment of inertia $\mathcal{I} = 10^{38}$ kg m^2 and distances to each target as listed in Tables 3 and 4.

As can be see in Figure 6, our observational ULs do not reach below the indirect energy constraint for any of the targets. While the sensitivity of O3 was improved over O2, none of the O3 targets had such a favorable combination of large frequency step size and small distance as the one from the Vela pulsar during O2 (Palfreyman 2016; Sarkissian et al. 2017; Palfreyman et al. 2018). Our closest result to the benchmark is for PSR J1105–6107, which had the second largest glitch of the selected targets in terms of $\Delta f_{\rm gl}/f$, and is at a closer distance and more favorable frequency than the only other target with a larger glitch (PSR J1826–1334). For this glitch, the closest the τ-dependent ULs get to the indirect energy constraint is within a factor of 1.6. As discussed, these empirical ULs are valid specifically for GW signals following the simple CW-like model of Equation (11), whereas many other models for GW emission following pulsar glitches are conceivable.

7. Conclusion

We have used data from the LIGO–Virgo observing run O3 to search for CW signals from 18 known pulsars, allowing for a mismatch between the frequencies of EM and GW emission, and for long-duration CW-like transients from six glitching pulsars. All statistically significant outliers were associated with instrumental disturbances and vetoed, and so we set ULs on the GW strain amplitude from each target.

The narrowband CW results obtained here complement the more constraining limits obtained from perfectly targeted searches on the same O3 data (Abbott et al. 2021e), where the GW frequency was assumed to be at exactly once or twice the EM-measured rotation frequency. With respect to the narrowband search done with the first half of O3 (Abbott et al. 2020b), we have improved our ULs by a factor of $\sim 35\%$ for PSR J0534+2200 and $\sim 10\%$ for PSR J0711–6830 and PSR J0835–4510, using respective parameter spaces ~ 6.5, 1.2, and 7.1 larger for these three pulsars. For the remaining pulsars, which were also searched for using the same method in O2, the limits presented here are a factor of 2–3 lower than those set in Abbott et al. (2019b). We surpass the spin-down limits for seven pulsars, including PSR J1105–6107 and PSR J1913+1011, for the first time using the narrowband method.

The best upper limit set across the whole frequency band is $h_0 \lesssim 2.3 \times 10^{-26}$ for PSR J0711–6830 at roughly 364 Hz using the 5n-vector search. We also set the best limit on pulsar ellipticity with PSR J0711–6830 at $\epsilon \lesssim 1.7 \times 10^{-8}$. However, neither of these limits surpass the indirect spin-down limits for this pulsar, which are a factor of ∼2.2 lower than the upper limits for the search. For pulsars with $h_0^{95\%} < h_{\rm sd}$, the best $h_0^{95\%}$ is $h_0 \lesssim 3.5 \times 10^{-26}$ for PSR J1913+1011 and the best ellipticity limit is $\epsilon \lesssim 2.7 \times 10^{-5}$ for PSR J0534+2200.

Our long-duration transient search results for signals following nine glitches in six pulsars significantly extend the target set for such searches over the two glitches from two pulsars previously covered with O2 data by Keitel et al. (2019), demonstrating the flexibility of the search method. We report two marginal outliers from the search for the last glitch of PSR J0537–6910 during O3, but do not consider them as significant detection candidates. We have set duration-dependent strain ULs for each post-glitch search and compared the results with the indirect glitch energy UL benchmark established in Prix et al. (2011), but have not reached this benchmark for any of these targets, with PSR J1105–6107 coming closest to it.

Although we do not explicitly show systematic error or statistical uncertainty on upper limits presented in Figures 1 and 6 or Table 2, their impact on these results is discussed here. Statistical uncertainty due to finite sampling when calculating limits is ∼3% for the $\mathcal{F}$-statistic CW search and 3%–5% for the post-glitch transient search. For the 5n-vector search, the uncertainty due to which part of the frequency band is sampled (i.e., typical distance from median UL across all 0.1 mHz sub-bands) is ∼2.4%. Meanwhile, the systematic error in the calibration of the O3 strain data is quantified in Sun et al. (2020, 2021) for LIGO and Acernese et al. (2022a) for Virgo. The error depends upon the time at which data were collected and upon the frequency band of the measurement. The maximum estimated systematic error in absolute magnitude of the strain across all frequencies and time is 7% for the LIGO detectors in O3a, 11% for the LIGO detectors in O3b, and 5% for Virgo, though typically the error is smaller than these levels. Additionally, calibration systematics are not correlated between detectors, and so it is likely that the absolute error in our combined measurements would be less than these values.

We expect that, with future upgrades of the LIGO–Virgo–KAGRA network (Abbott et al. 2020a), we can further improve GW results on the known pulsar population, and will be able to constrain emission scenarios and nuclear physics both for quiescent-state pulsars and those perturbed by glitches.

This material is based upon work supported by NSF's LIGO Laboratory, which is a major facility fully funded by the National Science Foundation. The authors also gratefully acknowledge the support of the Science and Technology Facilities Council (STFC) of the United Kingdom, the Max-Planck-Society (MPS), and the State of Niedersachsen/Germany for support of the construction of Advanced LIGO and construction and operation of the GEO 600 detector. Additional support for Advanced LIGO was provided by the Australian Research Council. The authors gratefully acknowledge the Italian Istituto Nazionale di Fisica Nucleare (INFN), the French Centre National de la Recherche Scientifique (CNRS), and the Netherlands Organization for Scientific Research (NWO), for the construction and operation of the Virgo detector and the creation and support of the EGO consortium. The authors also gratefully acknowledge research support from these agencies as well as by the Council of Scientific and Industrial Research of India, the Department of Science and Technology, India, the Science & Engineering Research Board (SERB), India, the Ministry of Human Resource Development, India, the Spanish Agencia Estatal de Investigación (AEI), the Spanish Ministerio de Ciencia e Innovación and Ministerio de Universidades, the Conselleria de Fons Europeus, Universitat i Cultura and the Direcció General de Política Universitaria i Recerca del Govern de les Illes Balears, the Conselleria d'Innovació Universitats, Ciència i Societat Digital de la Generalitat Valenciana and the CERCA Programme Generalitat de Catalunya, Spain, the National Science Centre of Poland and the European Union—European Regional Development Fund; Foundation for Polish Science (FNP), the Swiss National Science Foundation (SNSF), the Russian Foundation for Basic Research, the Russian Science Foundation, the European Commission, the European Social Funds (ESF), the European Regional Development Funds (ERDF), the Royal Society, the Scottish Funding Council, the Scottish Universities Physics Alliance, the Hungarian Scientific Research Fund (OTKA), the French Lyon Institute of Origins (LIO), the Belgian Fonds de la Recherche Scientifique (FRS-FNRS), Actions de Recherche Concertées (ARC) and Fonds Wetenschappelijk Onderzoek—Vlaanderen (FWO), Belgium, the Paris Île-de-France Region, the National Research, Development and Innovation Office Hungary (NKFIH), the National Research Foundation of Korea, the Natural Science and Engineering Research Council Canada, Canadian Foundation for Innovation (CFI), the Brazilian Ministry of Science, Technology, and Innovations, the International Center for Theoretical Physics South American Institute for Fundamental Research (ICTP-SAIFR), the Research Grants Council of Hong Kong, the National Natural Science Foundation of China (NSFC), the Leverhulme Trust, the Research Corporation, the Ministry of Science and Technology (MOST), Taiwan, the United States Department of Energy, and the Kavli Foundation. The authors gratefully acknowledge the support of the NSF, STFC, INFN, and CNRS for provision of computational resources.

This work was supported by MEXT, JSPS Leading-edge Research Infrastructure Program, JSPS Grant-in-Aid for Specially Promoted Research 26000005, JSPS Grant-in-Aid for Scientific Research on Innovative Areas 2905: JP17H06358, JP17H06361 and JP17H06364, JSPS Core-to-Core Program A. Advanced Research Networks, JSPS Grant-in-Aid for Scientific Research (S) 17H06133 and 20H05639, JSPS Grant-in-Aid for Transformative Research Areas (A) 20A203: JP20H05854, the joint research program of the Institute for Cosmic Ray Research, University of Tokyo, National Research Foundation (NRF), Computing Infrastructure Project of KISTI-GSDC, Korea Astronomy and Space Science Institute (KASI), and Ministry of Science and ICT (MSIT) in Korea, Academia Sinica (AS), AS Grid Center (ASGC) and the Ministry of Science and Technology (MoST) in Taiwan under grants including AS-CDA-105-M06, Advanced Technology Center (ATC) of NAOJ, and Mechanical Engineering Center of KEK.

We would like to thank all of the essential workers who put their health at risk during the COVID-19 pandemic, without whom we would not have been able to complete this work.

We acknowledge that CHIME is located on the traditional, ancestral, and unceded territory of the Syilx/Okanagan people. We are grateful to the staff of the Dominion Radio Astrophysical Observatory, which is operated by the National Research Council of Canada. CHIME is funded by a grant from the Canada Foundation for Innovation (CFI) 2012 Leading Edge Fund (Project 31170) and by contributions from the provinces of British Columbia, Québec, and Ontario. The CHIME/FRB Project, which enabled development in common with the CHIME/Pulsar instrument, is funded by a grant from the CFI 2015 Innovation Fund (Project 33213) and by contributions from the provinces of British Columbia and Québec, and by the Dunlap Institute for Astronomy and Astrophysics at the University of Toronto. Additional support was provided by the Canadian Institute for Advanced Research (CIFAR), McGill University, and the McGill Space Institute thanks to the Trottier Family Foundation, and the University of British Columbia. The CHIME/Pulsar instrument hardware was funded by NSERC RTI-1 grant EQPEQ 458893-2014. This research was enabled in part by support provided by WestGrid (www.westgrid.ca) and Compute Canada (www.computecanada.ca). We acknowledge support from the Natural Sciences and Engineering Research Council of Canada (NSERC) funding reference #CITA 490888-16, the Canadian Institute for Advanced Research, and the UBC Four Year Fellowship (6456).

We acknowledge support from EPSRC/STFC fellowship (EP/T017325/1), ANID/FONDECYT grants 1171421 and 1211964, and NASA grants 80NSSC19K1444 and 80NSSC21K0091. This work is supported by NASA through the NICER mission and the Astrophysics Explorers Program, and uses data and software provided by the High Energy Astrophysics Science Archive Research Center (HEASARC), which is a service of the Astrophysics Science Division at NASA/GSFC and High Energy Astrophysics Division of the Smithsonian Astrophysical Observatory.

Software: `Astropy` (Robitaille et al. 2013; Price-Whelan et al. 2018), `corner.py` (Foreman-Mackey 2016), `distromax` (Tenorio et al. 2021c, 2022), `GWpy` (Macleod et al. 2021), `LALSuite` (LIGO Scientific Collaboration 2021), `matplotlib` (Hunter 2007), `numpy` (Harris et al. 2020), `OctApps` (Wette et al. 2018b), `pandas` (McKinney 2010; Reback et al. 2020), `ptemcee` (Foreman-Mackey et al. 2013; Vousden et al. 2015), `PyFstat` (Ashton & Prix 2018; Ashton et al. 2021; Keitel et al. 2021), `scipy` (Virtanen et al. 2020), `SWIGLAL` (Wette 2020), `Tempo` (Nice et al. 2015), `Tempo2` (Edwards et al. 2006).

Appendix A
Differences in Pulsar Ephemerides Used for Different Pipelines

Due to variations in code infrastructure for the $\mathcal{F}$-statistic and 5n-vector pipelines, there were some cases where we used ephemerides with different parameterizations to search for the same source. In general, the `lalapps_Weave` code used for the $\mathcal{F}$-statistic CW search can search up to the fourth derivative in frequency, and the automatic template placement will work best if the reference time at which the frequency and spin-downs are defined is during or close to the time at which we are conducting the search. Similarly, the transient search (also based on the $\mathcal{F}$-statistic, but using the `lalapps_ComputeFstatistic_v2` code) can search up to $\ddot{f}$. On the other hand, the 5n-vector pipeline has no such limitations on the number of frequency derivatives.

In several cases, which we document below, the EM ephemerides used for the 5n-vector search included higher-order frequency derivatives to improve the phenomenological fit and reduce the effects of timing noise. In those cases, we refit the ephemerides using at most a fourth frequency derivative for the $\mathcal{F}$-statistic pipelines and we then used the simple heuristic from Equation (11) of Prix & Itoh (2005) to verify that the effect of the increased timing residuals on our matched-filter analysis was less than the maximum mismatch used to place templates for the search. The affected pulsars were:

1. PSR J0534+2200: The Crab pulsar was originally fit with 12 frequency derivatives, with an average timing residual of $\mathtt{TRES} = 135.0\ \mu$s, and this ephemeris was used for the 5n-vector search. For both $\mathcal{F}$-statistic-based pipelines we search with up to two frequency derivatives with an average timing residual of $\mathtt{TRES} = 482.382\ \mu$s.
2. PSR J0835–4510: The Vela pulsar was originally fit with seven frequency derivatives, with an average timing residual of $\mathtt{TRES} = 137.1\ \mu$s, and this ephemeris was used for the 5n-vector search. The $\mathcal{F}$-statistic CW pipeline ran with a search up to four frequency derivatives with an average timing residual of $\mathtt{TRES} = 133.2\ \mu$s.
3. PSR J1809–1917: This pulsar was originally fit with five frequency derivatives, with an average timing residual of $\mathtt{TRES} = 1766.4\ \mu$s, and this ephemeris was used for the 5n-vector search. The $\mathcal{F}$-statistic pipeline ran with a search up to four frequency derivatives with an average timing residual of $\mathtt{TRES} = 489.4\ \mu$s. In this case, it is likely that the timing residuals are smaller because the reference time used for the fits was moved to the middle of the observation time.

Appendix B
Settings for Background Estimation in $\mathcal{F}$-statistic Pipelines

B.1. CW Search

In this appendix, we outline the details of the method used for estimating the distribution of the expected largest outlier for the frequency-domain $\mathcal{F}$-statistic CW search. We then set a threshold corresponding to a p-value of 1% under the assumption that no signal is present in the data. We use the `distromax` method introduced by Tenorio et al. (2022), with some slight modifications due to the specific situation at hand.

We want to estimate the distribution of the maximum value of $2\mathcal{F}$ for the full search for a single pulsar, under the assumption that no signal is present. To be conservative, we will *exclude* bands corresponding to known disturbances when estimating this distribution, and as such we will have outliers that exceed our threshold to follow up that are associated with the disturbances. However, this means that we will not set our threshold accounting for the disturbances, which would generally push them upward and potentially cause a signal to be missed. The procedure is as follows:

1. Run the search and save the templates with the top 2×10^7 values of $2\mathcal{F}$.
2. Excise templates within the established width of known lines in Goetz et al. (2021); Piccinni et al. (2021).

3. Remove templates that are within $4 \times 10^{-5} f$ of unidentified lines, and in the case where the line is specified as "broad" in Goetz et al. (2021), we remove templates within $4 \times 10^{-4} f$.
4. Perform a single iteration of the notching procedure from Tenorio et al. (2022), which removes templates with a frequency within 5×10^{-5} Hz of any template exceeding an internal threshold.
5. Split the remaining $2\mathcal{F}$ values into 10^4 random batches of size $\sim 2 \times 10^3$. Find the maximum $2\mathcal{F}$ in each of those batches, and fit a Gumbel distribution to that set of maxima.
6. Propagate that Gumbel distribution based on the number of batches (Tenorio et al. 2022), and the *total* number of templates (i.e., the number of templates used before we perform notching, because this is the number of templates used to perform the search) to obtain a distribution for the maximum of the full search for that individual pulsar.

What is left is a distribution on the maximum value of $2\mathcal{F}$ under the assumption that no signal is present, and we can then integrate this distribution to find the value of $2\mathcal{F}$ that corresponds to a p-value of 1%. Any of the 2×10^7 original templates with $p < 1\%$ are then subject first to the vetoing procedure described in Section 4.3, and if they pass this procedure, then they are flagged for more extensive follow-up.

With the exception of one pulsar, PSR J1856+0245, the notching procedure above removes less than 40% of the frequency band. In the case of PSR J1856+0245, the known and unknown lines notching procedure removes the full frequency band, and so we do not search for CWs from this pulsar with the $\mathcal{F}$-statistic pipeline.

B.2. Transient Search

The basic approach for most targets in this analysis is the same as for the CW search, following the `distromax` method introduced by Tenorio et al. (2022): we fit a Gumbel distribution to the measured maxima of our detection statistic $B_{\mathrm{tS/G}}$ over random subsets ("batchmaxes"). We then propagate the parameters of this distribution considering the full number of templates. However, we then set the threshold less deep in the tails of the distribution than in the CW search, namely at the mean plus one standard deviation of the propagated Gumbel distribution. This same threshold is used both for candidate identification and later in the ULs procedure. The results from the seven transient searches where we apply this method are generally relatively clean, as indicated by the batchmax histograms and goodness of the Gumbel distribution fits, and so we do not employ any notching of disturbances across the board. However, for glitches 7 and 8 of PSR J0537–6910, additional features appear in the batchmax histograms and degrade the Gumbel fit. In both cases, with three iterations of the automated notching procedure from Tenorio et al. (2022), we can produce clean batchmax histograms. For glitch 7, the threshold on $B_{\mathrm{tS/G}}$ is quite robust under notching (changing from 11.3 to 11.0), and no outliers are recovered. On the other hand, for glitch 8, the threshold is lowered sufficiently (from 12.5 to 10.5), which reclassifies the largest values at two frequencies as marginal outliers. Follow-up of these outliers is detailed in Appendix D.

For PSR J1105–6107 and PSR J1826–1334, the number of templates is too small to obtain robust Gumbel fits with the `distromax` method. Instead, we use the off-sourcing approach (Isi et al. 2020): we indirectly estimate the background distribution by rerunning the full search 1000 times on different sky positions but with otherwise identical settings. This is feasible in these cases because the two searches are very cheap, i.e., less than a single core hour per run. By off-sourcing on the sky, we sample combinations of the same data that are statistically independent from the templates used in the main search. The practical implementation here matches that of Tenorio et al. (2021b): we keep decl. fixed and change only R.A. α, excluding a part of the sky closer than 0.5π to the pulsar in order to ensure statistical independence. We then fit a Gumbel distribution to the set of the highest $B_{\mathrm{tS/G}}$ values from each off-sourced search and again set the threshold at the mean plus one standard deviation of this distribution.

Appendix C
Follow-up of Remaining Outliers for CW Searches

In this section, we discuss follow-up of outliers found when searching in the direction of PSR J1838–0655 and PSR J1813–1749 (before glitch) with the $\mathcal{F}$-statistic. The same region of parameter space that produced outliers for PSR J1838–0655 in the $\mathcal{F}$-statistic search also produced outliers in the 5n-vector search.

The $\mathcal{F}$-statistic results of PSR J1813–1749, searching before the potential glitch, show an outlier at 44.62443216 Hz, close to a known line at H1 (see Figure 4). However, the outlier frequency is outside the nominal width of the line specified in Goetz et al. (2021), and is therefore unlikely to be caused by that specific artifact. On 16 April 2019, the frequencies of the calibration lines were changed to improve detector calibration, which altered the character of the persistent narrowband artifacts seen in H1 data (Sun et al. 2020). The known line in Figure 4 is an example of one such artifact. To test whether this candidate is caused by a separate but similar artifact, we run the search from the start of the run until only 16 April 16 2019. In Figure 7, by zooming in on the frequency range around the outliers, we show that quite a few templates have significantly higher values of $2\mathcal{F}$ than the outliers do for the full run. This behavior is inconsistent with a CW signal, and so we veto these outliers.

In Figure 3, we show that the outliers associated with PSR J1838–0655 are near an unknown disturbance at H1. The $2\mathcal{F}$ values running only on H1 data are larger for all of these candidates than they are when running on only L1 data, despite L1 being more sensitive in this frequency band. To test whether this is reasonable for a signal, we use the 1454 software injections that were detected above the search threshold when calculating ULs. We plot the $2\mathcal{F}$ calculated using L1 on the y-axis and $2\mathcal{F}$ calculated using H1 on the x-axis of Figure 8 for all injections (blue to yellow varied colors), and for the outliers (red). The dashed line indicates where these two values are equal. Only 2 out of 1454 injections cross the red line, meaning that if we veto any candidates to the right of the red line, we incur a false dismissal of 0.1%. Therefore, we veto this outlier in both the $\mathcal{F}$-statistic and the 5n-vector searches.

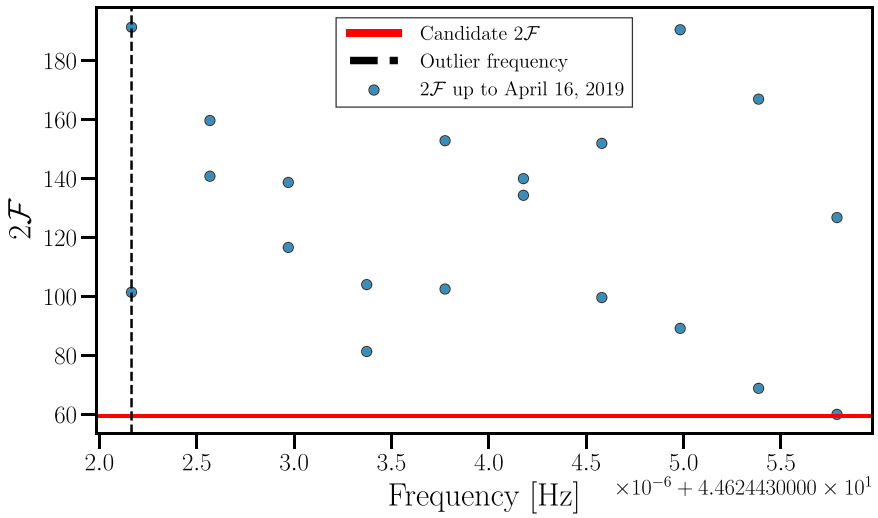

Figure 7. $2\mathcal{F}$ values vs. frequency (blue circles) for a search from 2019 April 1–2019 April 16 around the 44.62443216 Hz outlier in the $\mathcal{F}$-statistic search for PSR J1813–1749 bg. The red line indicates the $2\mathcal{F}$ value associated with the outlier, while the vertical black dashed line shows its frequency. It is clear that the search on just 2 weeks of data produces larger $2\mathcal{F}$ values than the search on the full year of data, which is inconsistent with a true signal. The data for this figure are available online (LIGO Scientific Collaboration et al. 2022).

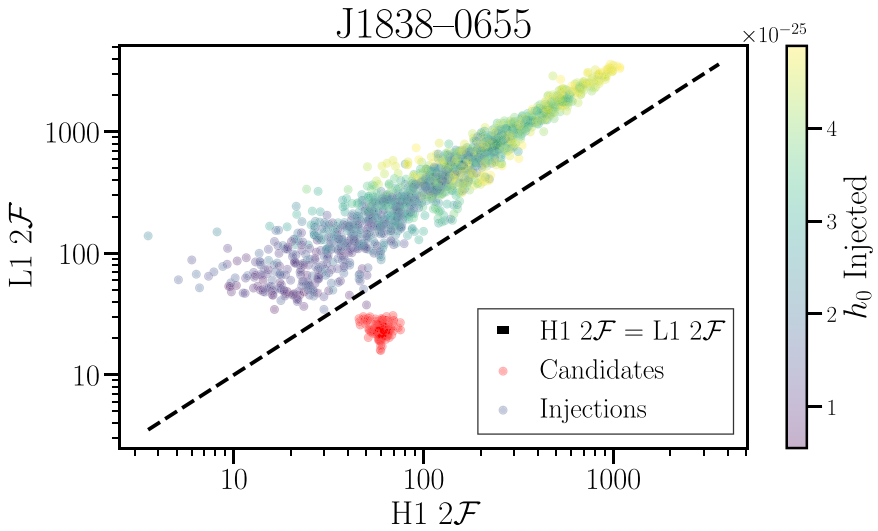

Figure 8. Individual detector $2\mathcal{F}$ values calculated for software injections detected when calculating ULs (blue to yellow dots indicating low to high h_0 injections), and outliers (red dots). The dashed line indicates where $2\mathcal{F}$ is equal for the two detectors. We see the red points clustered away from the software injections. Only two of the software injection recoveries fall on the right-hand side of the red line. The data for this figure are available online (LIGO Scientific Collaboration et al. 2022).

Appendix D
Follow-up of PSR J0537–6910 Glitch 8 Transient Search Outliers

Here, we discuss follow-up analyses of the marginal outliers recovered for the post-glitch transient search targeting glitch 8 of the Big Glitcher PSR J0537–6910. The parameters of the two outliers of interest are listed in Table 5. Another template with $B_{\mathrm{tS/G}}$ marginally above threshold is not offset by more than a single bin in any parameter from outlier A; we therefore do not follow that one up separately.

First, we checked for any evidence that the outliers may be caused by instrumental artifacts. There are no spectral artifacts of identified or unidentified origin listed in the relevant frequency band in Goetz et al. (2021) for LIGO nor in Piccinni et al. (2021) for Virgo. Comparing the time-frequency tracks of the outliers with single-detector spectrograms (Weldon et al. 2019) also reveals no suspicious structures. As a multidetector consistency check (Keitel et al. 2014; Leaci 2015), we recomputed the $\mathcal{F}_{mn}$ maps at each outlier's λ points for each individual detector. The corresponding max $2\mathcal{F}$ and $B_{\mathrm{tS/G}}$ values and best-fit (t_0, τ) pairs are collected in Table 6. Virgo does not recover these candidates, as expected because of its much lower sensitivity in this frequency range; instead, it returns unrelated short-duration peaks. But the H1 and L1 results are fully consistent with each other and with the multidetector result.

Other possible vetoes against an astrophysical origin include checking whether or not the detection statistics would increase when turning off Doppler modulation inside the $\mathcal{F}$-statistic code ("DMoff;" Zhu et al. 2017), or searching at a different sky position (off-sourcing; Isi et al. 2020). With a DMoff rerun of the full search band, we recover neither of the outliers as a local maximum, and the overall maximum at $\log_{10} B_{\mathrm{tS/G}} = 10.1143$ is lower, meaning that the outliers pass this check. For off-sourcing, we perform 1000 analyses at different α (at least 0.5π away from PSR J0537–6910) over 5 mHz wide sub-bands of the original search. This does not turn out to veto the outliers

Table 5
Outliers from the Transient Search after Glitch 8 of PSR J0537–6910

	f (Hz)	$\dot{f}$ (10^{-10} Hz s^{-1})	$\ddot{f}$ (10^{-20} Hz s^{-2})	$t_0^{\rm ML}$ (s)	$\tau^{\rm ML}$ (s)	max $2\mathcal{F}$	$\log_{10} B_{\rm tS/G}$	Tail Probability
A	123.7934283	−3.997	−8.39	1263844981	5209200	53.4	11.00	4%
B	123.8640925	−3.995	−1.89	1263628981	3913200	53.2	10.86	14%

Note. The transient parameter estimates $t_0^{\rm ML}$ and $\tau^{\rm ML}$ correspond to the location of the max $2\mathcal{F}$ value in the $\mathcal{F}_{mn}$ map. The posterior estimates (assuming flat priors, as for the $B_{\rm tS/G}$ statistic) are within 1 hour of the ML values—with the exception of τ for outlier A, which is about 7 hours longer than the ML value. The tail probability refers to the propagated Gumbel distribution following the `distromax` method with three notching iterations.

Table 6
Detector Consistency Follow-up for PSR J0537–6910 Glitch 8 Outliers

Detector(s)	$t_0^{\rm ML}$ (s)	$\tau^{\rm ML}$ (s)	max $2\mathcal{F}$	$\log_{10} B_{\rm tS/G}$	$t_0^{\rm MP}$ (s)	$\tau^{\rm MP}$ (s)
Outlier A						
HLV	1263844981	5209200	53.4	11.00	1263843607	5182844
H1	1263758883	5284800	29.0	5.14	1263758773	5217811
L1	1264317301	4669200	32.1	5.62	1263952957	5052102
V1	1252638018	57600	27.5	3.05	1240493379	282595
Outlier B						
HLV	1263628981	3913200	53.2	10.86	1263628503	3912769
H1	1263629283	2196000	31.2	4.80	1263629183	2197636
L1	1263590101	3945600	33.6	5.27	1263589393	4108995
V1	1240437618	3600	28.3	2.95	1247483923	5400

Note. These values are all obtained from the $\mathcal{F}_{mn}$ maps evaluated at the λ parameters as listed for each outlier in Table 5. The transient parameter estimates $t_0^{\rm ML}$ and $\tau^{\rm ML}$ correspond to the location of the max $2\mathcal{F}$ value, while $t_0^{\rm MP}$ and $\tau^{\rm MP}$ are maximum-posterior estimates.

either, as we do not find extended sets of similar or larger $B_{\rm tS/G}$ values at many other sky positions and similar frequencies, as could be expected from some types of instrumental artifacts. However, we can once again fit a Gumbel distribution to the maxima of these off-sourced searches and propagate to the corresponding expected distribution over the whole search bank while taking into account the missing trials factor of 25. This results in tail probabilities of 2% and 3% for the two outliers, which are lower than the 4% and 14% from `distromax` but still above the 1% threshold used by the two CW search pipelines.

We also followed up both outliers with four separate pipelines: (i) gridless follow-up with `PyFstat` (Ashton & Prix 2018; Ashton et al. 2021; Keitel et al. 2021; Tenorio et al. 2021b); (ii) the $\mathcal{F}$-statistic CW pipeline using `lalapps_Weave`, as described in Section 4.3; (iii) the 5n-vector method as described in Section 4.2; and (iv) the targeted time-domain Bayesian method (Dupuis & Woan 2005; Pitkin et al. 2017), as also used for the targeted searches in Abbott et al. (2021e). In (i), we use the same implementation of the transient $\mathcal{F}$-statistic as in the main search. But for (ii)–(iv), we treat the candidates as putative CW signals of fixed length, fixing the start time t_0 and end time $t_0 + \tau$ of these analyses based on the outlier parameters from Table 5.

The `PyFstat` package (Ashton et al. 2021; Keitel et al. 2021) contains an implementation of Markov Chain Monte Carlo (MCMC) gridless follow-up (Ashton & Prix 2018; Tenorio et al. 2021b) using the `ptemcee` sampler (Foreman-Mackey et al. 2013; Vousden et al. 2015) and the same $\mathcal{F}$-statistic code in `LALSuite` (Wette 2020; LIGO Scientific Collaboration 2021). We do not employ this here as a veto or for significance estimation, but only to check that the candidates can be recovered independently of the original search grid setup, when putting Gaussian priors on the λ parameters around their previously recovered values, and now also allowing variations in sky position. These `PyFstat` analyses recover consistent max $2\mathcal{F}$ values and locations.

The `lalapps_Weave` pipeline also uses the same underlying $\mathcal{F}$-statistic implementation. The main difference is that this method does not search over different signal start times and durations; instead, the start time t_0 and end time $t_0 + \tau$ are fixed, and it only searches over the λ parameters. As expected, this follow-up recovers $\mathcal{F}$-statistic peaks consistent with the outlier parameters.

With the 5n-vector method and a similar follow-up setup as for `lalapps_Weave`, we again recover local peaks at the frequency of each outlier. But over the given data span, this follow-up also recovers other peaks with higher S-statistic values across the probed 0.45 Hz bands and spin-down ranges. Thus, it does not confirm the outliers as candidates of interest. For outlier A, there are 15 peaks with higher detection statistic (corresponding to 0.36% of the top level candidates in every 10^{-4} Hz sub-band and marginalized over the spin-down region). For outlier B, there are five peaks with higher detection statistics (0.15% of the top level candidates in every 10^{-4} Hz sub-band and spin-down region).

Finally, the targeted time-domain Bayesian method fixes the signal duration as well as the λ parameters, and performs nested sampling over the four amplitude parameters $\mathcal{A}$. For both outliers, this returned Bayes factors of about 500 in favor of a coherent signal in all three detectors, as opposed to noise or incoherent signals in the individual detectors. However, this fully targeted analysis does not provide any additional assessment of statistical significance. In addition, the estimated strain amplitudes h_0 from this follow-up, $4.5^{+1.5}_{-1.4} \times 10^{-26}$ and $5.2^{+1.7}_{-1.7} \times 10^{-26}$ at 95% credible intervals, are a factor of 10

above the indirect glitch energy UL from Equation (12) assuming a signal from PSR J0537–6910 and with the NICER-observed glitch size.

ORCID iDs

A. Basu https://orcid.org/0000-0002-4142-7831
I. Cognard https://orcid.org/0000-0002-1775-9692
K. Crowter https://orcid.org/0000-0002-1529-5169
C. M. L. Flynn https://orcid.org/0000-0003-1110-0712
E. Fonseca https://orcid.org/0000-0001-8384-5049
D. C. Good https://orcid.org/0000-0003-1884-348X
L. Guillemot https://orcid.org/0000-0002-9049-8716
S. Guillot https://orcid.org/0000-0002-6449-106X
M. J. Keith https://orcid.org/0000-0001-5567-5492
J. W. McKee https://orcid.org/0000-0002-2885-8485
B. W. Meyers https://orcid.org/0000-0001-8845-1225
R. M. Shannon https://orcid.org/0000-0002-7285-6348
B. Shaw https://orcid.org/0000-0002-9581-2452
I. H. Stairs https://orcid.org/0000-0001-9784-8670
B. W. Stappers https://orcid.org/0000-0001-9242-7041
C. M. Tan https://orcid.org/0000-0001-7509-0117
G. Theureau https://orcid.org/0000-0002-3649-276X
P. Weltevrede https://orcid.org/0000-0003-2122-4540

References

Aasi, J., Abadie, J., Abbott, B. P., et al. 2014, ApJ, 785, 119
Aasi, J., Abbott, B. P., Abbott, R., et al. 2015a, CQGra, 32, 074001
Aasi, J., Abbott, B. P., Abbott, R., et al. 2015b, PhRvD, 91, 022004
Aasi, J., Abbott, B. P., Abbott, R., et al. 2015c, ApJ, 813, 39
Abbott, B. P., Abbott, R., Abbott, T. D., et al. 2017a, ApJ, 839, 12
Abbott, B. P., Abbott, R., Abbott, T. D., et al. 2017b, PhRvD, 96, 122006
Abbott, B. P., Abbott, R., Abbott, T. D., et al. 2018, PhRvL, 120, 031104
Abbott, B. P., Abbott, R., Abbott, T. D., et al. 2019a, ApJ, 879, 10
Abbott, B. P., Abbott, R., Abbott, T. D., et al. 2019b, PhRvD, 99, 122002
Abbott, B. P., Abbott, R., Abbott, T. D., et al. 2019c, ApJ, 875, 122
Abbott, B. P., Abbott, R., Abbott, T. D., et al. 2020a, LRR, 23, 3
Abbott, B. P., Abbott, R., Adhikari, R., et al. 2007, PhRvD, 76, 082001
Abbott, B. P., Abbott, R., Adhikari, R., et al. 2008, ApJL, 683, L45
Abbott, R., Abbott, T. D., Abraham, S., et al. 2020b, ApJL, 902, L21
Abbott, R., Abbott, T. D., Abraham, S., et al. 2021a, PhRX, 11, 021053
Abbott, R., Abbott, T. D., Abraham, S., et al. 2021b, ApJL, 913, L27
Abbott, R., Abbott, T. D., Abraham, S., et al. 2021c, ApJ, 922, 71
Abbott, R., Abbott, T. D., Abraham, S., et al. 2021d, PhRvD, 103, 064017
Abbott, R., Abbott, T. D., Acernese, F., et al. 2022, PhRvD, 105, 022002
Abbott, R., Abe, H., Acernese, F., et al. 2021e, arXiv:2111.13106
Acernese, F., Agathos, M., Agatsuma, K., et al. 2015, CQGra, 32, 024001
Acernese, F., Agathos, M., Aiello, L., et al. 2019, PhRvL, 123, 231108
Acernese, F., Agathos, M., Ain, A., et al. 2022a, CQGra, 39, 045006
Acernese, F., Agathos, M., Ain, A., et al. 2022b, arXiv:2203.04014
Amiri, M., Bandura, K. M., Boyle, P. J., et al. 2021, ApJS, 255, 5
Anderson, P. W., & Itoh, N. 1975, Natur, 256, 25
Arzoumanian, Z., Baker, P. T., Blumer, H., et al. 2020, ApJL, 905, L34
Ashok, A., Beheshtipour, B., Papa, M. A., et al. 2021, ApJ, 923, 85
Ashton, G., Keitel, D., Prix, R., & Tenorio, R. 2021, PyFstat, v1.11.6, Zenodo, doi:10.5281/zenodo.4688639
Ashton, G., & Prix, R. 2018, PhRvD, 97, 103020
Astone, P., Colla, A., D'Antonio, S., et al. 2014, PhRvD, 89, 062008
Astone, P., Colla, A., D'Antonio, S., Frasca, S., & Palomba, C. 2012, JPhCS, 363, 012038
Astone, P., D'Antonio, S., Frasca, S., & Palomba, C. 2010, CQGra, 27, 194016
Astone, P., Frasca, S., & Palomba, C. 2005, CQGra, 22, S1197
Bailes, M., Jameson, A., Abbate, F., et al. 2020, PASA, 37, e028
Bailes, M., Jameson, A., Flynn, C., et al. 2017, PASA, 34, e045
Bandura, K., Addison, G. E., Amiri, M., et al. 2014, Proc. SPIE, 9145, 914522
Basu, A., Shaw, B., Antonopoulou, D., et al. 2022, MNRAS, 510, 4049
Bennett, M. F., van Eysden, C. A., & Melatos, A. 2010, MNRAS, 409, 1705
Buikema, A., Cahillane, C., Mansell, G. L., et al. 2020, PhRvD, 102, 062003
Camilo, F., Ransom, S. M., Halpern, J. P., & Roshi, D. A. 2021, ApJ, 917, 67
Covas, P. B. 2020, MNRAS, 500, 5167
Cutler, C., & Schutz, B. F. 2005, PhRvD, 72, 063006
Davis, D., Massinger, T. J., Lundgren, A. P., et al. 2019, CQGra, 36, 055011
Davis, D., Areeda, J. S., Berger, B. K., et al. 2021, CQGra, 38, 135014
Dodson, R., Legge, D., Reynolds, J. E., & McCulloch, P. M. 2003, ApJ, 596, 1137
Dunn, L., Lower, M. E., & Melatos, A. 2021, MNRAS, 504, 3399
Dupuis, R. J., & Woan, G. 2005, PhRvD, 72, 102002
Edwards, R. T., Hobbs, G. B., & Manchester, R. N. 2006, MNRAS, 372, 1549
Espinoza, C. M., Lyne, A. G., Stappers, B. W., & Kramer, M. 2011, MNRAS, 414, 1679
Fesik, L., & Papa, M. A. 2020, ApJ, 895, 11
Foreman-Mackey, D. 2016, JOSS, 1, 24
Foreman-Mackey, D., Hogg, D. W., Lang, D., & Goodman, J. 2013, PASP, 125, 306
Fuentes, J. R., Espinoza, C. M., Reisenegger, A., et al. 2017, A&A, 608, A131
Gendreau, K. C., et al. 2016, Proc. SPIE, 9905, 420
Glampedakis, K., & Gualtieri, L. 2018, Astrophys. Space Sci. Libr, 457, 673
Goetz, E., Neunzert, A., Riles, K., et al. 2021, O3a Lines and Combs Found in Self-gated C01 Data, Tech. Rep., LIGO-T2100200, LIGO Laboratory
Goncharov, B., Shannon, R. M., Reardon, D. J., et al. 2021, ApJL, 917, L19
Gotthelf, E. V., & Halpern, J. P. 2008, ApJ, 681, 515
Halpern, J. P., Camilo, F., Gotthelf, E. V., et al. 2001, ApJL, 552, L125
Harris, C. R., Millman, K. J., van der Walt, S. J., et al. 2020, Natur, 585, 357
Haskell, B. 2017, in Proc. IAU. 13, Symp. 337, Pulsar Astrophysics—The Next 50 Years, ed. P. Weltevrede et al. (Cambridge: Cambridge Univ. Press), 203
Haskell, B., & Melatos, A. 2015, IJMPD, 24, 1530008
Haskell, B., & Schwenzer, K. 2020, in Handbook of Gravitational Wave Astronomy, ed. C. Bambi, S. Katsanevas, & K. D. Kokkotas (Singapore: Springer), 1
Ho, W. C. G., Espinoza, C. M., Antonopoulou, D., & Andersson, N. 2015, SciA, 1, e1500578
Ho, W. C. G., Espinoza, C. M., Arzoumanian, Z., et al. 2020a, MNRAS, 498, 4605
Ho, W. C. G., Guillot, S., Saz Parkinson, P. M., et al. 2020b, MNRAS, 498, 4396
Hobbs, G. B., Manchester, R. N., & Toomey, L. 2021, The Australia Telescope National Facility Pulsar Catalogue: Glitch Parameters, https://www.atnf.csiro.au/people/pulsar/psrcat/glitchTbl.html
Hunter, J. D. 2007, CSE, 9, 90
Isi, M., Mastrogiovanni, S., Pitkin, M., & Piccinni, O. J. 2020, PhRvD, 102, 123027
Jankowski, F., Bailes, M., van?Straten, W., et al. 2018, MNRAS, 484, 3691
Jaranowski, P., Królak, A., & Schutz, B. F. 1998, PhRvD, 58, 063001
Kaplan, D. L., Chatterjee, S., Gaensler, B. M., & Anderson, J. 2008, ApJ, 677, 1201
Keitel, D., & Ashton, G. 2018, CQGra, 35, 205003
Keitel, D., Prix, R., Papa, M. A., Leaci, P., & Siddiqi, M. 2014, PhRvD, 89, 064023
Keitel, D., Tenorio, R., Ashton, G., & Prix, R. 2021, JOSS, 6, 3000
Keitel, D., Woan, G., Pitkin, M., et al. 2019, PhRvD, 100, 064058
Kramer, M., & Wex, N. 2009, CQGra, 26, 073001
Lattimer, J. M., & Prakash, M. 2004, Sci, 304, 536
Leaci, P. 2015, PhyS, 90, 125001
LIGO Scientific Collaboration 2021, LIGO Algorithm Library—LALSuite, Free Software (GPL), doi:10.7935/GT1W-FZ16
LIGO Scientific Collaboration, Virgo Collaboration, & KAGRA Collaboration 2022, Data Release for Narrowband Searches for Continuous and Long-duration Transient Gravitational Waves from known Pulsars in the LIGO-Virgo Third Observing Run, Tech. Rep., LIGO-G2102435, LIGO Laboratory
Lindblom, L., & Owen, B. J. 2020, PhRvD, 101, 083023
Link, B., Epstein, R. I., & Lattimer, J. M. 2000, in Stellar Astrophysics—Proc. Pacific Rim Conf., ed. K. S. Cheng et al. (Dordrecht: Springer), 117
Link, B., Epstein, R. I., & Van Riper, K. A. 1992, Natur, 359, 616
Lorimer, D. R., & Kramer, M. 2012, Handbook of Pulsar Astronomy (Cambridge: Cambridge Univ. Press)
Lower, M. E., Johnston, S., Dunn, L., et al. 2021, MNRAS, 508, 3251
Lower, M. E., Bailes, M., Shannon, R. M., et al. 2019, RNAAS, 3, 192
Lower, M. E., Bailes, M., Shannon, R. M., et al. 2020, MNRAS, 494, 228
Lyne, A. G., Shemar, S. L., & Smith, F. G. 2000, MNRAS, 315, 534
Macleod, D. M., Areeda, J. S., Coughlin, S. B., Massinger, T. J., & Urban, A. L. 2021, SoftX, 13, 100657

Manchester, R. N., Hobbs, G. B., Teoh, A., & Hobbs, M. 2005, AJ, 129, 1993
Mastrogiovanni, S., Astone, P., D'Antonio, S., et al. 2017, CQGra, 34, 135007
McKinney, W. 2010, in Proc. 9th Python in Science Conf., ed. S. van der Walt & J. Millman (Austin, TX: SciPy), 56
Melatos, A., Douglass, J. A., & Simula, T. P. 2015, ApJ, 807, 132
Middleditch, J., Marshall, F. E., Wang, Q. D., Gotthelf, E. V., & Zhang, W. 2006, ApJ, 652, 1531
Nice, D., Demorest, P., Stairs, I., et al. 2015, Tempo: Pulsar Timing Data Analysis, Astrophysics Source Code Library, ascl:1509.002
Nieder, L., Clark, C. J., Kandel, D., et al. 2020, ApJL, 902, L46
Palfreyman, J. 2016, ATel, 9847, 1
Palfreyman, J., Dickey, J. M., Hotan, A., Ellingsen, S., & van Straten, W. 2018, Natur, 556, 219
Piccinni, O., Janssens, K., Fiori, I., et al. 2021, Virgo O3 List of Lines, Tech. Rep., LIGO-T2100141-v2, LIGO Laboratory
Pietrzyński, G., Graczyk, D., Gallenne, A., et al. 2019, Natur, 567, 200
Pitkin, M., Isi, M., Veitch, J., & Woan, G. 2017, arXiv:1705.08978v1
Price-Whelan, A. M., Sipőcz, B. M., Günther, H. M., et al. 2018, AJ, 156, 123
Prix, R. 2007, PhRvD, 75, 023004
Prix, R. 2009, in Neutron Stars and Pulsars, ed. W. Becker (Berlin: Springer), 651
Prix, R. 2015, The F-statistic and its Implementation in ComputeFStatistic_v2, Tech. Rep., LIGO-T0900149, LIGO Laboratory
Prix, R., Giampanis, S., & Messenger, C. 2011, PhRvD, 84, 023007
Prix, R., & Itoh, Y. 2005, CQGra, 22, S1003
Reardon, D. J., Shannon, R. M., Cameron, A. D., et al. 2021, MNRAS, 507, 2137
Reback, J., Mendel, B., McKinney, W., et al. 2020, pandas-dev/pandas: Pandas, v1.1.2, Zenodo, doi:10.5281/zenodo.4019559
Robitaille, T. P., Tollerud, E. J., Greenfield, P., et al. 2013, A&A, 558, A33
Sarkissian, J. M., Reynolds, J. E., Hobbs, G., & Harvey-Smith, L. 2017, PASA, 34, e027
Shaw, B., Keith, M. J., Lyne, A. G., et al. 2021, MNRAS, 505, L6
Shaw, B., Lyne, A. G., Mickaliger, M. B., et al. 2021, Jodrell Bank Pulsar Glitch Catalogue, http://www.jb.man.ac.uk/pulsar/glitches.html
Sieniawska, M., & Bejger, M. 2019, Univ, 5, 217
Singh, A. 2017, PhRvD, 95, 024022
Sun, L., Goetz, E., Kissel, J. S., et al. 2020, CQGra, 37, 225008
Sun, L., Goetz, E., Kissel, J. S., et al. 2021, arXiv:2107.00129
Tenorio, R., Keitel, D., & Sintes, A. M. 2021a, Univ, 7, 474
Tenorio, R., Keitel, D., & Sintes, A. M. 2021b, PhRvD, 104, 084012
Tenorio, R., Modafferi, L. M., Keitel, D., & Sintes, A. M. 2021c, distromax, v1.0.4, Zenodo, doi:10.5281/zenodo.5779414
Tenorio, R., Modafferi, L. M., Keitel, D., & Sintes, A. M. 2022, PhRvD, 105, 044029
Trimble, V. 1973, PASP, 85, 579
Vajente, G., Huang, Y., Isi, M., et al. 2020, PhRvD, 101, 042003
van Eysden, C. A., & Melatos, A. 2008, CQGra, 25, 225020
Verbiest, J. P. W., Lentati, L., Hobbs, G., et al. 2016, MNRAS, 458, 1267
Verbiest, J. P. W., Weisberg, J. M., Chael, A. A., Lee, K. J., & Lorimer, D. R. 2012, ApJ, 755, 39
Viets, A., & Wade, M. 2021, Subtracting Narrow-band Noise from LIGO Strain Data in the Third Observing Run, Tech. Rep., LIGO-T2100058, LIGO Laboratory
Virtanen, P., Gommers, R., Oliphant, T. E., et al. 2020, NatMe, 17, 261
Vousden, W. D., Farr, W. M., & Mandel, I. 2015, MNRAS, 455, 1919
Weldon, G., Riles, K., & Team, L. I. G. O. 2019, APS Meeting Abstracts, 2019, Y10.007
Wette, K. 2014, PhRvD, 90, 122010
Wette, K. 2020, SoftX, 12, 100634
Wette, K., Walsh, S., Prix, R., & Papa, M. A. 2018a, PhRvD, 97, 123016
Wette, K., Prix, R., Keitel, D., et al. 2018b, JOSS, 3, 707
Wette, K., Owen, B. J., Allen, B., et al. 2008, CQGra, 25, 235011
Wex, N., & Kramer, M. 2020, Univ, 6, 156
Yao, J. M., Manchester, R. N., & Wang, N. 2017, ApJ, 835, 29
Yim, G., & Jones, D. I. 2020, MNRAS, 498, 3138
Yu, M., Manchester, R. N., Hobbs, G., et al. 2013, MNRAS, 429, 688
Zhu, S. J., Papa, M. A., & Walsh, S. 2017, PhRvD, 96, 124007
Zweizig, J., & Riles, K. 2021, Information on Self-gating of h(t) Used in O3 Continuous-wave and Stochastic Searches, Tech. Rep., LIGO-T2000384, LIGO Laboratory